Characterization of benthic communities at Loki's Castle vent field using a photomosaic

Ida Marie Hamstad

Thesis for the degree
Master of Science in Marine Biology
University of Bergen

Supervisors: Pedro Ribeiro, Mari Heggernes Eilertsen & Thibaut Barreyre

August, 2021

Abstract

Loki's Castle was the first black smoker hydrothermal vent field to be discovered on the Arctic Mid-Ocean Ridge (AMOR), and is known to host a specialized and highly endemic fauna. Despite being studied since its discovery in 2008 there are still knowledge gaps, especially regarding the diversity and spatial distribution of the faunal community. The increasing interest in opening areas at the AMOR to deep sea mining makes it crucial to gather baseline data from the sites that could be affected, including Loki's Castle. The purpose of this thesis was to characterize the abundance, diversity and spatial distribution of the benthic megafauna community at Loki's Castle and to investigate the influence of abiotic factors on this community. To achieve this, an ortophotomosaic created from seafloor images of the area was used to annotate and quantify all visible fauna. These observations were analyzed together with pre-existing data of abiotic parameters (temperature and heat flux) and topographic variables (slope, aspect and roughness) from the vent field, using a multivariate analytical framework. A total of 14743 observations were recorded, and 20 morphospecies belonging to eight different phyla were identified. There were statistically significant differences between diffuse venting areas, focused venting areas and peripheral areas in density, diversity and morphospecies distribution. The diffuse venting site called the Barite field supports a diverse and dense community of organisms. Some of these, such as the tubeworm *Sclerolinum contortum*, are dependent on symbiosis with chemosynthetic bacteria, while others are likely influenced by a facilitating cascade where *S. contortum* is the primary foundation species. Temperature and slope were found to significantly influence the spatial distribution of most of the prominent morphospecies, total abundance and species richness. However, most of the species distributions could not be explained by temperature and slope, and it is likely that other biological and abiotic factors such as food availability, competition, predation, substrate and hydrothermal fluid composition also contribute to the observed patterns. This hypothesis should be investigated in future experimental studies. A seabed mining event at or near Loki's Castle could change the benthic megafaunal community through elimination of vital habitat and alteration of the hydrothermal circulation from vents. This thesis provides baseline knowledge that can be useful in assessing how the benthic megafaunal community will be impacted by a possible future mining event.

Acknowledgements

First of all I want to extend my sincerest gratitude to my supervisors for all your guidance, help and support during the work on this thesis. Pedro Ribeiro, thank you for all your guidance and enthusiasm throughout this project. I appreciate that you always took the time to explain the things I didn't understand, answered any questions I had, and gave me thorough feedback on my manuscript. Mari Eilertsen, thank you for the help with faunal identifications and for very helpful revisions of the manuscript. Your faunal knowledge has been invaluable. Dr. Thibaut Barreyre, thank you for providing the photomosaics that made this thesis possible and for providing insights about the geological aspects of Loki's Castle.

I am very grateful to Rasmus Rikter-Svendsen for kindly providing the observations of *Sclerolinum contortum* and temperature and heat flux data. I would also like to thank Aino Hosia from the University Museum of Bergen for help with identifications of the two jellyfish and the ctenophore, and Nicolas Straube, also from the University Museum, for help with the identification of *Rhodichtys regina*.

Lastly, I would like to thank my friends and family. I would not have been able to complete this thesis without your continuous support.

Ida Marie Hamstad
30. August, 2021

Contents

1. Introduction

1.1 Hydrothermal vents

The deep sea, defined as the part of the ocean below 200 meters depth, makes up 95% of the inhabitable volume of the biosphere (Levin, 2019), but remains the least explored biome of Earth (Danovaro *et al.*, 2020). These depths accommodate a fauna that clearly differs from the fauna in shallower waters (Tyler, 2003). Our view of the deep sea has changed radically during the last decades as a result of extensive scientific exploration. It is no longer seen as a cold and dark place with poor diversity, but rather a large ecosystem hosting a range of habitats and diverse faunal communities (Ramirez-Llodra *et al.*, 2010; Levin, 2019). The discovery of hydrothermal vents in 1977 has in particular contributed to this change (Van Dover *et al.*, 2020). Today, we know about 600 hydrothermal vents in the world, and there are probably more to be discovered (Boschen *et al.*, 2013). Although hydrothermal vents are small habitats that make up only $50km^2$ of the oceans, they are ecologically important and shed light on the origins on life on Earth and possible life on other planets (Van Dover *et al.*, 2018; Schulte, 2007). The unique biodiversity endemic to these extreme environments also provide new opportunities for bioprospecting and biodiscovery (Stokke *et al.*, 2020).

Hydrothermal vents are found along all mid-ocean ridges, as well as on back-arc spreading centers and some seamounts (Van Dover *et al.*, 2002). They form as a result of geophysical reactions in tectonically active areas of the seafloor. Cold seawater enters cracks in the seafloor and is heated up by the hot magma underneath, accumulating metal sulphides from the seafloor rock in the process (Petersen *et al.*, 2016). As the water becomes less dense and rises, it exits as hydrothermal fluids that can reach up to 400°C. The metal sulphides precipitate and form chimneys ("black smokers" and "white smokers"), mounds and plumes (Petersen *et al.*, 2016). About half of the hydrothermal fluid does not emanate from the chimneys, but mixes with seawater and exits as a low temperature (<20°C) fluid, in a process known as diffuse venting (Ramirez-Llodra *et al.*, 2007; Jamieson & Gartman, 2020).

The geophysical processes that control seafloor spreading determine the rate of spreading and extent of hydrothermal venting in a particular area (Tunnicliffe *et al.*, 2003). The spreading rates at mid-ocean ridges differ greatly, from superfast spreading ridges (130-170mm $yr^{-}1$) such as the East Pacific Ridge, to ultraslow spreading ridges (<20mm $yr^{-}1$) such as the Arctic Mid-Ocean Ridge (Ramirez-Llodra *et al.*, 2007). Even though fast spreading ridges in general have more vent fields than ultraslow spreading ridges, ultraslow spreading ridges can also facilitate extensive venting (Pedersen *et al.*, 2010). Vents at slow-spreading ridges are situated further away from each other, are less subject to natural disturbances, and generally longer-lived than vents at fast-spreading ridges (Mullineaux *et al.*, 2018). Ultraslow ridges make up 20% of the global ridge system, but are not well studied (Pedersen *et al.*, 2010).

1.1.1 Chemosynthetic based ecosystems (CBEs)

The discovery of hydrothermal vents was the first discovery of an ecosystem that was supported by chemical energy instead of sunlight (Tunnicliffe *et al.*, 2003). At the basis of this food chain are chemoautotrophic microorganisms, who use chemosynthesis for primary production instead of photosynthesis. Similar chemosynthesis-based ecosystems (CBEs) can be found at cold seeps and organic falls. Cold seeps are found on both active and passive continental margins, and emit fluids that have high methane concentrations and are at about the same temperature as the surrounding seawater (Sibuet & Olu, 1998). Organic falls, such as whale carcasses, wood logs and kelp, are food sources in the deep sea that attract a range of species (Baco & Smith, 2003; Bienhold *et al.*, 2013). The degradation processes at these sites create high concentrations of sulfide and methane, which are utilized by chemoautotrophic bacteria (Treude *et al.*, 2009; Bienhold *et al.*, 2013).

These unique ecosystems have gained wide interest because of their possible links to the very first ecosystems on Earth, as well as to extraterrestrial ecosystems (Schulte, 2007; Nakamura & Takai, 2014). At hydrothermal vents, the hot hydrothermal fluids are rich in reduced chemicals such as hydrogen, hydrogen sulfide, iron and methane, and create a chemical disequilibrium upon mixing with the seawater (Sievert & Vetriani, 2012). It is this disequilibrium that is utilized by the chemoautotrophic microorganisms for primary production, transferring the energy to higher trophic levels (Sievert & Vetriani, 2012).

1.1.2 Hydrothermal vent biota

Vent-specific species depend on chemoautotrophic productivity, and need to be able to live in the extreme and highly varying physical conditions of the vent environment (Desbruyères *et al.*, 2006). Many vent species host chemosynthetic microorganisms as either epi- or endosymbionts, while others act as grazers of the microbial mats (Van Dover *et al.*, 2002). Species living in vent environments have developed physiological and behavioral adaptations to be able to withstand the extreme physical conditions that characterize the vent area, such as high temperature, low oxygen levels and toxic substances (McMullin *et al.*, 2007). Some benthic vent species can tolerate temperatures over 50°C and a pH of 5 (Lee, 2003; McMullin *et al.*, 2007).

Hydrothermal vent ecosystems typically have high endemism, low diversity, and very high biomass compared to the surrounding deep sea (Ramirez-Llodra *et al.*, 2007). These patterns reflect the high energy availability at hydrothermal vents, as well as the extreme ranges of environmental conditions (e.g. very high to very low temperatures) (Ramirez-Llodra *et al.*, 2007). Over 640 vent species (not including microbes) have been described so far (Chapman *et al.*, 2019), and on average two new discoveries are made every month (Ramirez-Llodra *et al.*, 2007). Arthropods, molluscs and annelids are among the most common phyla at hydrothermal vents (Ramirez-Llodra *et al.*, 2007). The vent-specific fauna differs from the community of background fauna that lives in proximity of the vents (Boschen *et al.*, 2013). The hard substrate megafauna living around vents are commonly sessile, filter-feeding, long-lived and slow-growing, and benefit from the enhanced food supply at vent sites (Galkin, 1997; Erickson *et al.*, 2009; Boschen *et al.*, 2013). Typical taxa include anemones, sponges and hydroids (Galkin, 1997; Boschen *et al.*, 2013).

The heterogenous nature of vent sites create a complex mosaic of habitats for vent-specific and background fauna to inhabit (Bernardino *et al.*, 2012). Abiotic factors, such as the distance to fluid exit and distribution of oxygen, iron and sulphur, have shown to be important in shaping vent species distributions (Luther *et al.*, 2001; Cuvelier *et al.*, 2009; Gerdes *et al.*, 2019). The flux and concentrations of vent fluids create gradients that often correlate with the distribution of species (Mullineaux *et al.*, 2018). However, biological interactions such as predation can also affect the community structure at hydrothermal vents (Micheli *et al.*, 2002). In addition, foundation species such as tubeworms create habitats that contribute in shaping the faunal community (Portail *et al.*, 2015).

1.1.3 Connectivity and biogeography

Most vent-associated species rely on the conditions and chemoautotrophic primary production at hydrothermal vents, and are only able to survive in habitats with these conditions (Desbruyères *et al.*, 2006). Hydrothermal vents are scarce and unevenly distributed (Tunnicliffe *et al.*, 2003), and may be separated by a few kilometers up to several hundred kilometers (Mullineaux *et al.*, 2018). Thus, larvae of vent-specific animals often have to cross large areas of unsuitable habitat to be able to disperse to a new vent site (Tyler & Young, 2003; Adams *et al.*, 2012). Long distances between suitable sites can be barriers to dispersal, and there are also physical barriers, such as elevated sections of mid-ocean ridges (Van Dover *et al.*, 2002). Knowledge on population connectivity for hydrothermal vent species is limited, especially for background species (Klunder *et al.*, 2020).

Population persistence, colonization of new vents, and recolonization of disturbed vents all depend on larval dispersal (Adams *et al.*, 2012). A species dispersal potential depends on both biotic and abiotic factors, where planktonic larval duration seems to be particularly important for vent species (Mullineaux *et al.*, 2018). There have only been studies on planktonic larval duration for a few vent species, and these have shown durations from 6 weeks to 3 months (Marsh *et al.*, 2001; Watanabe *et al.*, 2004; Mullineaux *et al.*, 2018). Genetic connectivity studies show that deep sea taxa in general disperse longer distances than shallow water species, although there are large differences between species (Baco *et al.*, 2016).

Dispersal abilities differ between taxa and are influenced by species-specific life histories and behaviors (Vrijenhoek, 2010). Studies have shown that some species are able to disperse to vents several hundred kilometers away (Mullineaux *et al.*, 2010). However, dispersal over long distances likely requires intermediate habitats that act as stepping stones (Breusing *et al.*, 2016). Species living on hard substrate, in demersal or in pelagic habitats seem to be able to disperse further than species living on soft-bottom (Baco *et al.*, 2016). Some vent populations can also be connected with populations from other chemosynthetic ecosystems, such as seeps and organic falls (Portail *et al.*, 2015; Eilertsen *et al.*, 2017).

On a global scale, hydrothermal vents can be divided into five different biogeographical provinces; Mid-Atlantic Ridge, Indian Ocean, Western Pacific, Northeast Pacific, and East Pacific Rise, each with an unique fauna (Moalic *et al.*, 2012). It is also proposed that the Arctic might make up a sixth biogeographic province (Van Dover *et al.*, 2002). The species

endemism is high – 95% of species are only found within one province (Moalic *et al.*, 2012). The fauna can also be considerably different between vent sites within the same region (Van Dover *et al.*, 2018), and the connectivity within a region is related to the distance between vent habitats (Mullineaux *et al.*, 2018). In addition to dispersal barriers, habitat suitability and disturbance frequency is contributing to the differences between vents and regions (Goffredi *et al.*, 2017; Mullineaux *et al.*, 2018).

1.2 Threats to conservation

The deep sea is under increasing threat from several anthropogenic stressors, including climate change, hydrocarbon extraction, seabed mining, deep-sea fisheries, pollution and litter (Danovaro *et al.*, 2020). The deep sea absorbs large amounts of heat and CO_2 from the atmosphere, making it a crucial contributor in slowing climate change and regulating the climate on Earth (Levin & Le Bris, 2015). These mechanisms expose the vulnerable deep-sea ecosystems to increasing stress, triggering physical and ecological consequences yet poorly understood (Levin & Le Bris, 2015). Increased uptake of CO_2 by the ocean lowers the pH of seawater and leads to ocean acidification, and by 2100 the pH of seawater could decrease by 0.4-0.5 units (Caldeira & Wickett, 2003; Ramirez-Llodra *et al.*, 2011). This would be critical for calcifying species, who have skeletons or shells that contain calcium carbonate (Caldeira & Wickett, 2003). Increased temperature in the ocean may affect the global ocean circulation and create more oxygen minimum zones in the deep sea (Keeling *et al.*, 2010). Oxygen minimum zones are characterized by reduced biomass, diversity and body size for calcifying species, crustaceans and fish (Ramirez-Llodra *et al.*, 2011).

Anthropogenic stressors co-occur and will have cumulative impacts on the ecosystems in the deep sea (Ramirez-Llodra *et al.*, 2011). As a result, life-supporting services such as the biological pump and nutrient cycling could be altered (Danovaro *et al.*, 2017). The limited area of suitable habitat for the specialized hydrothermal vent fauna, means that even a small disturbance could possibly cause regional extinction in these habitats (Levin, 2019). Alterations of the specific oceanographic and geochemical conditions that vent fauna depend on could especially affect the community (Levin, 2019). Increasing industrial activity can degrade deep-sea ecosystems where we still have little knowledge about their biological diversity (Danovaro *et al.*, 2020).

An emerging threat to hydrothermal vent ecosystems is deep-sea mining. The seafloor massive sulfide (SMS) deposits that often form from hydrothermal activity contain valuable metals such as zinc, lead, cadmium, copper, silver and gold (Ramirez-Llodra *et al.*, 2011; Petersen *et al.*, 2016). This has made vent sites attractive for mining, especially in the last few years as the need for metals for green technology is growing (Levin, 2019). With recent technological improvements and increased mineral prices, deep-sea mining is about to become economically viable (Boschen *et al.*, 2013), and the whole ocean floor is thought to have metal reserves that are over 600 times larger than the reserves on land (Cathles, 2011). Hydrothermal vents, however, are small in size, and only a few of the known vent sites have reserves that are large enough and of sufficient grade to sustain multi-year mining (Hannington & Monecke, 2009; Petersen *et al.*, 2016). However, SMS mining targeting inactive vents could have serious consequences for nearby active vents (Van Dover *et al.*, 2018; Van Dover, 2019), as well as to other vulnerable ecosystems in the vicinity of mining operation.

Deep-sea mining is a new type of stress for hydrothermal vent communities, and comes on top of the stress from other anthropogenic impacts. Since no commercial seabed mining has commenced yet, there is still little evidence of how vent communities will respond to this disturbance (Van Dover *et al.*, 2018). At the mining site itself, substrate and fauna would suffer physical destruction, hydrothermal circulation might be altered (Jamieson & Gartman, 2020), and there are possible indirect effects of sediment plumes and dissolved metals (Ramirez-Llodra *et al.*, 2011). Communities at nearby active vents could also be indirectly affected by this plume (Van Dover *et al.*, 2020). After a disturbance event, the benthic community composition at a hydrothermal vent could be altered for decades, with variable ability to recover between different taxa (Gollner *et al.*, 2017). Recovery of communities at slow spreading ridges might be slower than communities at fast spreading ridges, due to the relatively lower frequency of natural disturbances at these sites (Gollner *et al.*, 2017). In order to implement appropriate management strategies, there is an urgent need to gain knowledge about the impacts deep sea mining could have on the vent fauna (Boschen *et al.*, 2013).

The International Seabed Authority (ISA) regulates the opening of areas to mining in waters outside national jurisdiction, commonly called "the Area" (Dunn *et al.*, 2018). There are currently 30 contracts for exploration activities issued by the ISA, but no actual mining operations have started (International Seabed Authority, 2021). 42% of the favorable areas for seafloor massive sulphides (SMS) are however located inside Exclusive Economic Zones

(Petersen *et al.*, 2016). In Norway, the new "Law on Mineral Activities on the Continental Shelf" was approved in July 2019, stating that areas on the Norwegian continental shelf can be opened for mining activity (Seabed Mineral Law, 2019). The law also states that an environmental impact assessment (EIA) has to be carried out before mining activity can be allowed in a certain area. Within Norwegian waters, the Arctic-Mid Ocean Ridge has been pointed out as a potential source for seabed minerals (Pedersen & Bjerkgård, 2016; Ramirez-Llodra *et al.*, 2020), and SMS deposits are likely the mineral resource generating most economic interest in Norway.

1.3 The Arctic Mid-Ocean Ridge

The Arctic Mid-Ocean Ridge (AMOR) stretches 4000km from the northern shelf of Iceland to the Siberian Shelf (Baumberger *et al.*, 2016), with large parts laying within Norwegian waters (Pedersen & Bjerkgård, 2016). The ridge system consists of six different segments with different characteristics (Pedersen & Bjerkgård, 2016). It is a ultraslow spreading ridge with spreading rates varying between 18mm yr-1 and 12.7mm yr-1 (Dick *et al.*, 2003). Located at a bend where the Mohn's ridge meets the Knipovich ridge, we find the hydrothermal vent field known as Loki's Castle (Pedersen *et al.*, 2010), which is the study area of this thesis.

1.3.1 Loki's Castle vent field

Loki's Castle vent field (LCVF) was first discovered in July 2008 during a UiB-led research cruise to the AMOR (Pedersen *et al.*, 2010), at a depth of 2350m (Kongsrud & Rapp, 2012). The vent field was at first difficult to find, and hence got its name from the Norse god Loki, who was a shapeshifter and a trickster (Baumberger *et al.*, 2016). The discovery was unique because this was not only the first black smoker vent field to be discovered on the Arctic ridge system, but also the first black smoker vent field to be discovered on an ultraslow spreading ridge (Pedersen *et al.*, 2010).

The four active black smoker chimneys are located at two hydrothermal sulfide mounds that are approximately 150m apart (Baumberger *et al.*, 2016). The western mound contains three of the chimneys; Sleepy, Menorah and Camel, while the fourth chimney, João, is located at the eastern mound (Rikter-Svendsen, 2020). The chimneys are up to 13 meters tall, and emit hydrothermal fluids up to 320°C (Pedersen et al. 2010). Near the eastern mound there is

a barite field, characterized by barite structures covered with microbial mats and diffuse, low-temperature (<20°C) venting (Steen et al. 2016). Colonies of *Sclerolinum contortum* are also abundant in this area. North of the barite field is an area called the Oasis, with diffuse venting and large colonies of the tube worm *S. contortum* and bacterial mats (Rikter-Svendsen, 2020). White bacterial mats are present in both the high temperature and low temperature areas (Tandberg *et al.*, 2012).

Despite being located at one of Earth's slowest spreading ridge segments (Baumberger *et al.*, 2016), Loki's Castle shows considerable venting and has an unusually large hydrothermal deposit (Pedersen *et al.*, 2010). The hydrothermal circulation at the site is influenced by sediment from the nearby Bear Island sediment fan, even though the site itself is not covered by sediment (Baumberger *et al.*, 2016). Because of the sediment influence, the hydrothermal fluids contain an unusual high amount of reduced chemical compounds (Jaeschke *et al.*, 2012). The Jan Mayen vent field further south on the Mohn's ridge does not show such high concentrations (Olsen *et al.*, 2015). The hydrothermal fluid of Loki's Castle is especially rich in methane, hydrogen and ammonium, and is further characterized by a pH of 5.5 (Pedersen *et al.*, 2010). The CO_2 concentration is also very high compared to the surrounding seawater (Olsen *et al.*, 2015).

The high amount of reduced chemical compounds provides energy for a range of different chemosynthetic microorganisms (Jaeschke *et al.*, 2012). The black smoker chimneys are covered by Epsilonbacteria of the genus Sulfurovum, while the bacterial mats in the barite area are dominated by Epsilonbacteria of the genus Sulfurimonas (Steen *et al.*, 2016). Methane and hydrogen sulfide are important electron donors in both high and low temperature areas, and in addition hydrogen is important in the high temperature area (Steen *et al.*, 2016). Completely new lineages of microorganisms have been found at AMOR, which provide great opportunities for bioprospecting (Stokke *et al.*, 2020). The high activity by chemosynthetic microorganisms are important energy sources for the community of invertebrates inhabiting the vent site.

1.3.2 Fauna at Loki's Castle

The deep-sea fauna at Loki's Castle vent site is unique, specialized and differs from a typical Atlantic vent fauna (Pedersen *et al.*, 2010). Tube-building polychaetes, melitid amphipods and gastropods are highly present in the community (Kongsrud & Rapp, 2012). The fauna

differs between the high temperature venting areas and the diffuse, low temperature venting areas. The high temperature venting areas are characterized by low biomass and diversity, and a highly varying abundance (Tandberg *et al.*, 2018). The black smoker chimney walls have a high amount of small grazing gastropods (Pedersen *et al.*, 2010), and amphipods are also common here (Tandberg *et al.*, 2018). The soft bottom of the diffuse venting areas facilitates a diverse and abundant fauna, and is dominated by dense fields of *S. contortum* and other tube-dwelling polychaetes such as *Nicomache lokii*, in addition to gastropods and amphipods (Pedersen *et al.*, 2010; Kongsrud & Rapp, 2012; Tandberg *et al.*, 2018).

Eleven species of amphipods from five different families, and fourteen species of polychaetes have been identified in samples from Loki's Castle (Kongsrud *et al.*, 2017; Tandberg *et al.*, 2018), but no species inventory for this locality has yet been published. The tube-dwelling polychaetes *N. lokii* and *S. contortum* create dense mats that provide three-dimensional habitat for other invertebrates as well as help to stabilize the soft sediments, and are considered keystone species of the ecosystem (Pedersen *et al.*, 2010; Kongsrud & Rapp, 2012). The amphipod *Themisto abyssorum* is considered to be an important predator in the ecosystem, and its prey consists of micro-eukaryotes, metazoans and detritus (Olsen *et al.*, 2014).

A high proportion of the species found at Loki's Castle are endemic (Pedersen *et al.*, 2010; Kongsrud *et al.*, 2017). The amphipods *Exitomelita sigynae* and *Monoculodes bousfieldi* are found inhabiting the black smoker chimney walls and the low venting area, and are so far only known from Loki's Castle (Tandberg *et al.*, 2012, 2018). Other endemic species include two species of tube-building polychaetes from the family Ampharetidae (Kongsrud *et al.*, 2017). However, the knowledge about the fauna at Loki's Castle is limited, and more species are likely to be identified as the site is studied further. Furthermore, very little is known about spatial distribution patterns and their possible relationship with environmental conditions, particularly hydrothermal venting.

1.3.3 Connectivity

The Arctic Ocean is relatively isolated and the deep sea fauna have a high proportion of endemic species (Svavarsson *et al.*, 1993; Stuart & Rex, 2009). Characteristic species of the Mid-Atlantic Ridge, such as mussel beds and alvinocarid shrimps are not present at AMOR (Schander *et al.*, 2010), and there are no known shared species between AMOR vents and MAR vents (M. Eilertsen, personal communication). Iceland separates AMOR from the

Mid-Atlantic Ridge, and acts as a barrier for dispersal and migration between the two ridge systems (Sweetman *et al.*, 2013).

The specialized fauna at Loki's Castle differs from the fauna at shallow hydrothermal vents further south on the Mohn's ridge (Kongsrud *et al.*, 2017). These white smoker vents at approximately 500m to 700m depth contain very few vent-endemic species (Schander *et al.*, 2010). The benthic fauna is also very different from the inactive sulfide mound Mohn's Treasure located 30 km south of Loki's Castle (Ramirez-Llodra *et al.*, 2020). The pelagic eukaryotic microorganisms at Loki's Castle are affected by depth and venting, and differs from the pelagic community in the surrounding water masses (Olsen *et al.*, 2015). The community of pelagic eukaryotes shows a different diversity than the communities at Jan Mayen vent fields (Olsen *et al.*, 2014).

There are indications that some of the species at Loki's Castle could have migrated from nearby cold seep environments (Pedersen *et al.*, 2010). The polychaetes *S. contortum* and *N. lokii* are found both at Loki's Castle and at the cold seep habitat Håkon Mosby mud volcano (Eilertsen *et al.*, 2018). It is proposed that the fauna found at Loki's Castle is a combination of migration from cold seeps in the Arctic and local adaptation (Pedersen *et al.*, 2010). However, there is still missing knowledge about faunal composition and connectivity at AMOR vent sites (Ramirez-Llodra *et al.*, 2020).

1.4 Aim and structure of thesis

The increasing interest in opening areas to deep sea mining, both internationally and in Norwegian waters, makes it crucial to gather baseline data from the relevant sites that may be directly or indirectly impacted by mining operations (Ramirez-Llodra *et al.*, 2020). Since the discovery of Loki's Castle in 2008, there has been extensive research on the site and its associated fauna. Despite this, there are still important knowledge gaps regarding its biodiversity. Moreover, the spatial distribution of faunal assemblages and the relationship between those assemblages and the local abiotic conditions has not yet been studied. The aim of this thesis is to characterize the diversity, distribution and abundance of the benthic megafauna at Loki's Castle hydrothermal vent field in relation to hydrothermal activity. To this purpose I used an ortophotomosaic created from seafloor images of the area to annotate and quantify all visible fauna. Biological observations were then integrated with pre-existing data regarding the characteristics and distribution of hydrothermal outflow across Loki's

Castle vent field (Rikter-Svendsen, 2020). A multivariate analytical framework was then used to investigate the existence of distinctive faunal assemblages across Loki's Castle, and a possible correlation with hydrothermal characteristics.

2. Methods

2.1 Study site

The study site for this thesis is the Loki's Castle vent field located on the Mohn-Knipovich bend of the Arctic Mid-Ocean Ridge (Figure 2.1). A description of the environmental and biological characteristics of this site is provided in the Introduction section.

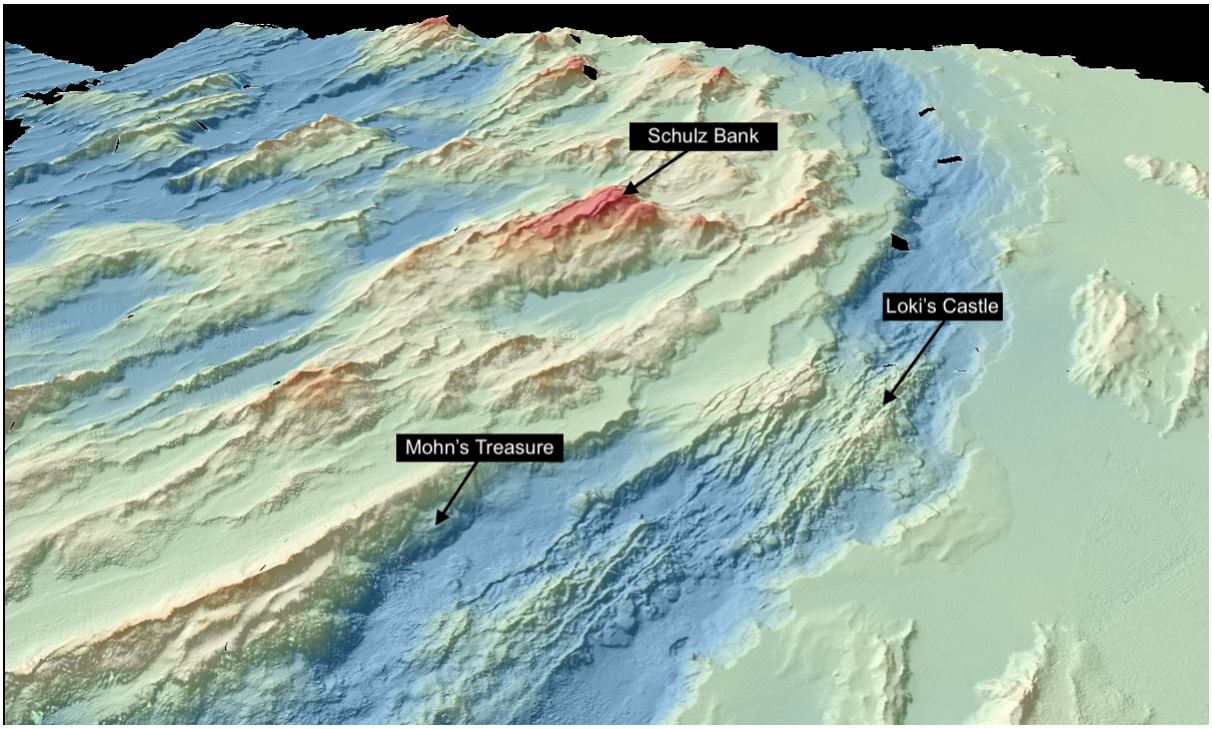

Figure 2.1: Map showing the location of Loki's Castle on the Arctic Mid-Ocean Ridge (courtesy of Jon Thomassen Hestetun, NORCE Research Centre). The map was generated from bathymetry data available at *http://dybdedata.no*.

2.2 Data collection

Image data were gathered from two remotely operated vehicle (ROV) photographic surveys conducted at the Loki's Castle vent field in 2018 (Rikter-Svendsen, 2020). The survey was conducted by the K.G. Jebsen Centre for Deep Sea Research aboard R/V G. O. Sars, using ROV Ægir 6000. Both surveys operated at an altitude of approximately 4m above the seafloor and a speed of 0.13m/s (Rikter-Svendsen, 2020). Survey 1 covered the Eastern mound and the Barite field (Figure 2.2) and was approximately 10 hours long, while survey 2 covered the Western mound and lasted for approximately 2.5 hours (Rikter-Svendsen, 2020). Both surveys captured images at a frequency of one photo every 15 seconds, using a DSC 24,000 digital still camera that was attached vertically on the ROV (Rikter-Svendsen, 2020). This resulted in 2617 images from survey 1, and 657 images from survey 2.

2.3 Mosaic creation

Two high-resolution photomosaics (one for each ROV survey) were created from the images in a previous study (see Rikter-Svendsen (2020) for full details), and kindly provided by Dr. Thibaut Barreyre.The mosaic of Loki East covers an area of 13336 m^2, comprising one sulphide mound and the associated black smoker chimney João, and two diffuse venting areas termed as barite field and oasis (Figure 2.2). The mosaic of Loki West covers an area of 4227,6 m^2 and includes one sulphide mound with the active black smoker chimneys Sleepy, Menorah and Camel. Before the creation of the photomosaics, the images were pre-processed. This included correcting for uneven illumination, equalizing overall intensity of the images and correcting geometrical distortion from the camera lenses (Barreyre *et al.*, 2012; Rikter-Svendsen, 2020). Vehicle navigation data were used to align the images, along with feature-matching of the seafloor structures between both consecutive and non-consecutive images (Escartín *et al.*, 2008). The images were further adjusted by scaling and rotating. Blending and color correction were performed to create a seamless photomosaic (Barreyre *et al.*, 2012; Rikter-Svendsen, 2020).

2.4 Mosaic annotation

The software MosaicViewer (Girona Underwater Vision and Robotics, 2014) was used to annotate all visible fauna on the photomosaics, by visualizing and extracting positioning data

from the mosaic through creating points, lines and polygons with UTM coordinates (Girona Underwater Vision and Robotics, 2014). All visible fauna were marked as points and identified to the lowest taxon possible. As is common in image analysis of benthic communities, many observations could not be identified to species level. The term morphospecies was therefore applied throughout this thesis, meaning that animals with similar morphological characteristics were grouped together, and assigned open nomenclature terms. As recommended by Horton *et al.* (2021), the abbreviation "indet." was applied when further identification was not possible from images alone, and "stet." was applied when the animal was not identified further because of lack of taxonomic expertise.

The largest megafauna (fish, anemones, shrimp) was visible from the mosaic and marked directly in the mosaic. The smaller fauna was identified by opening the high-resolution raw images within MosaicViewer, and their approximate position was marked in the mosaic. Observations (as polygons) of *S. contortum* colonies were kindly provided by Rasmus Rikter-Svendsen. Lists of fauna observations with UTM coordinates were exported as text files for further analysis on a Geographical Information System.

2.5 QGIS and spatial analysis

Spatial analysis of the data was carried out in the open source geographic information system QGIS 3.18 (QGIS Development Team, 2009). Faunal observations from the photomosaics were projected as vector points onto a bathymetry map of Loki's Castle with a grid resolution of 20 x 5 cm. Total numbers and densities for each morphotype were calculated based on the area of each photomosaic. Average temperature and heat flux data, obtained by Rikter-Svendsen (2020), were added as raster files with 5 x 5 m pixel resolution (see Appendix A). Using *"vector research tools"* in QGIS, a grid with squares of 5 x 5 m was made to match the pixels of the temperature data.

The number of individuals of each morphotype within each grid cell was calculated with the QGIS tool *"count points in polygon"*. For colonies of *S. contortum*, the percentage coverage within each grid cell was estimated by intersecting the polygons with the grid layer. The resulting layers with counts of individuals per morphotype and coverage of *S. contortum* were converted to raster files by using the QGIS tool *"rasterize"*. Slope, roughness and aspect were calculated from the bathymetry map using raster analysis, and the average within each grid cell was then calculated with the tool *"raster layer zonal statistics"*. All raster values were sampled, and the data were exported as text files for multivariate statistical analysis.

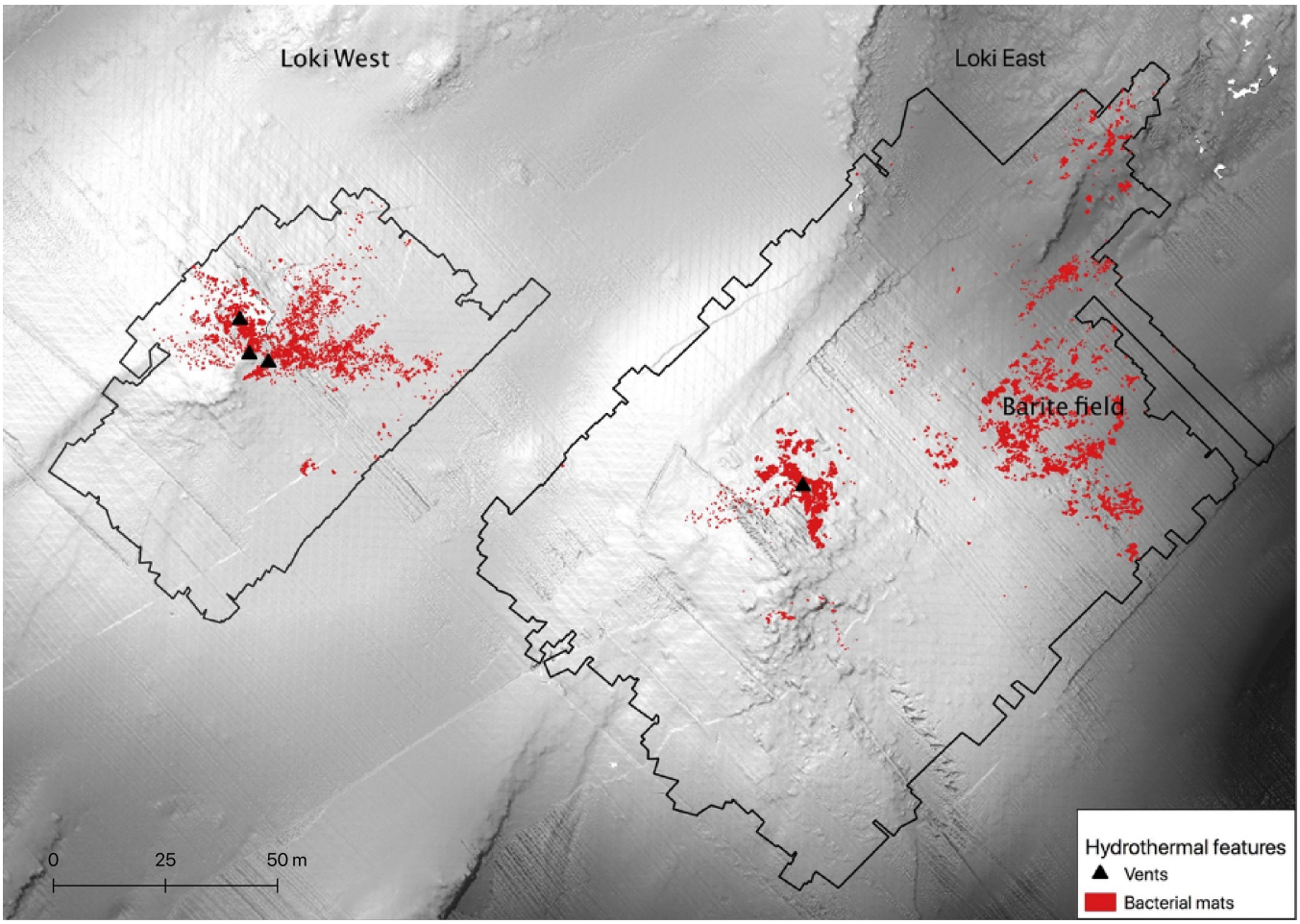

Figure 2.2: Boundaries (black lines) of the two photomosaics covering Loki East and Loki West.

2.6 Delimitation of study sites

Study sites were delimited based on temperature measurements and geographic position. Grid cells with an average temperature that was measurably different from the ambient seawater were designated as three study sites based on geographic proximity: The Western mound, the Eastern mound, and the Barite field (Figure 2.3). The area earlier referred to as the Oasis was included in the study site called the Barite field. This was done on the basis of the abiotic similarity of the two areas (T. Barreyre, personal communication) and the fact that they are adjacent to each other. All grid cells where the average temperature did not measurably differ from the surrounding seawater were termed as the Western and Eastern periphery.

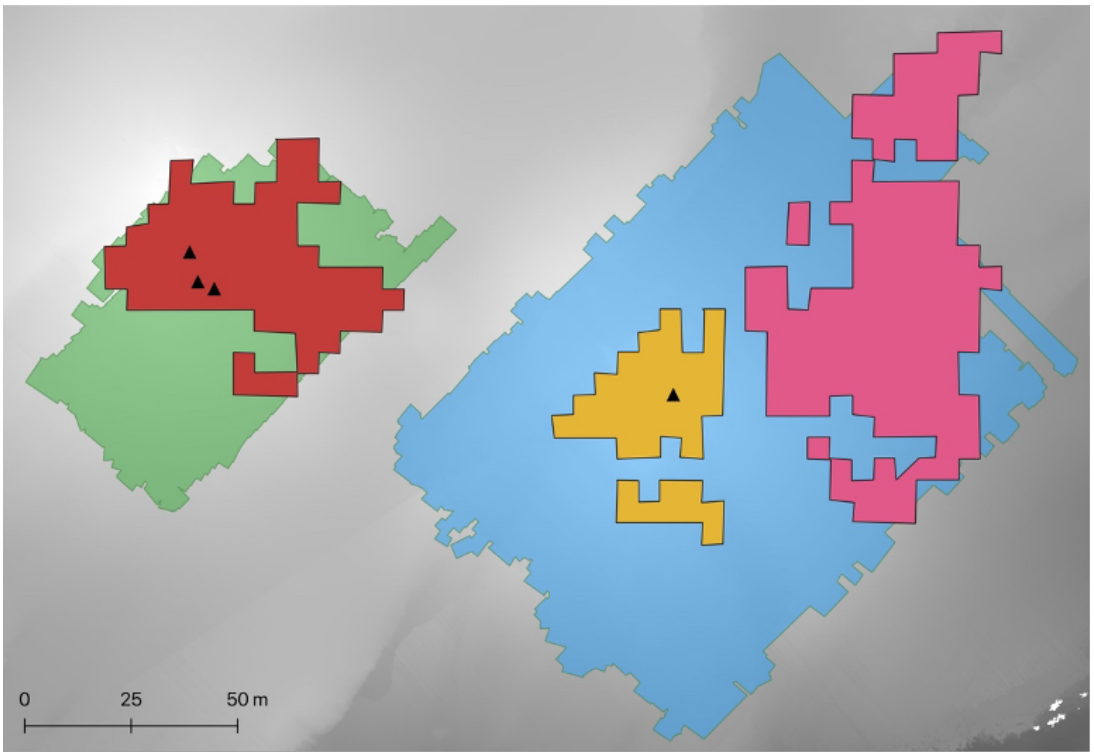

Figure 2.3: The study sites at Loki's Castle: Western mound (red), Eastern mound (yellow), Barite field (pink), Western periphery (green), and Eastern periphery (blue). Active vents are marked as triangles.

2.7 Statistical analysis

All statistical analyses were conducted in R version 3.5.2 (R Development Core Team, 2010) within the RStudio IDE version 1.1.463 (RStudio Team, 2016).The full reproducible code is provided in Appendix B. A statistical significance level (alpha) of 0.05 was used for all statistical tests. All plots were produced with the package *ggplot2* (Wickham, 2016).

Mean and standard error of total density per morphospecies were calculated for each study site using the package *dplyr* (Wickham *et al.*, 2015). For *S. contortum*, the average coverage per m^2 was calculated instead of density. To be able to compare density between sites, a relative total density was calculated for each site using square root transformed data. The proportion of morphospecies at each study site was calculated, this was also based on square root transformed densities (coverage for *S. contortum*) for comparison between sites.

Species diversity was calculated for each grid cell as the number of species (S), Shannon diversity index (H), and the inverse Simpson diversity index (1/D), using the *"diversity"*

function from the *vegan* package, which provides tools for descriptive community ecology (Oksanen *et al.*, 2013). Pielou's evenness (J) were calculated by J=H/ln(S). *S. contortum* was not included in the calculation of diversity indices (except the number of species) since diversity indices are calculated from abundances, and the data for *S. contortum* were expressed as coverage. For each study site the mean and standard error of the diversity indices were calculated using the *dplyr* package.

Kruskal-Wallis tests were performed to test differences in biological indices between the sites. The Kruskal-Wallis test was chosen instead of ANOVA because the data had a non-normal distribution and non-homogeneity of variance. This was tested first with Shapiro-Wilk tests and Levene's tests. A post-hoc Dunn's test from the package *dunn.test* was applied to test pairwise differences in biological diversity indices between study sites (Dinno, 2017).

A nMDS plot was made from a Bray-Curtis dissimilarity matrix to visualize any difference in morphospecies composition between the study sites. The Bray-Curtis dissimilarity matrix was made from the *vegan* function *"vegdist"*. The nMDS analysis was done with the function *"metaMDS"*, which also performs a Wisconsin double transformation and square root transformation on the data prior to the analysis. The *"metaMDS"* function was run with three dimensions, 999 maximum iterations and 500 maximum numbers of random starts.

A Permutational multivariate analysis of variance (PERMANOVA) with 999 permutations was used to test whether the groups indicated by the nMDS were statistically significant. This was done with the *"adonis"* function from the vegan package, on the Wisconsin and square root transformed Bray-Curtis dissimilarity matrix. The function *"pairwiseAdonis"* (Martinez Arbizu, 2020) was then applied to test which sites were statistically different. A Similarity Percentage (SIMPER) analysis, also from the *vegan* package, assessed which morphospecies contributed the most to the dissimilarity between sites, caused by variation in species abundances.

To test correlations between abiotic factors and morphospecies, a Spearmans' rank correlation coefficient matrix was made using the function *"rcorr"* from the *Hmisc package* (Harrell Jr, 2019). Spearman's correlation measures the monotonic association between two variables and was chosen because not all variables showed a linear relationship. Only the eight most common morphospecies were included in the matrix. Aspect was divided into Northness (cos(aspect)) and Eastness (sin(aspect)).

Generalized additive models (GAMs) were performed to test the effect of abiotic factors on total abundance (N), number of species (S), and the most common morphotypes. GAMs were chosen to be able to model non-linear relationships between response and predictor variables (Jones & Wrigley, 1995). Only temperature and slope were included as predictor variables in the model, both containing a smoothing function. Heat flux was not included because it showed very high concurvity with temperature, and roughness was not included as it showed very high concurvity with slope. Concurvity is the non-parametric equivalent to multicollinearity, and if present it can make the fitted parameter estimates of the GAM highly unstable (Ramsay *et al.*, 2003). Northness and Eastness was not included because they did not show significant Spearman's rank correlations with the morphospecies.

3. Results

3.1 Faunal observations

A total of 14743 observations were recorded, and 20 morphospecies were identified (Figure 3.1). The observations were distributed across eight phyla, namely Porifera, Cnidaria, Ctenophora, Mollusca, Annelida, Arthropoda, Echinodermata, and Chordata (Table 3.1). Five of the morphospecies were pelagic and highly mobile, while the rest were benthic. Of these, seven were mobile and eight were sessile. Cnidaria was the most diverse phylum with five morphospecies, followed by Porifera with four morphospecies. Actiniaria stet. 2 was the morphospecies with most observations, 4935 in total. This was over twice as much as the morphospecies with second most observations, Actiniaria stet. 1 with 2140 observations. Other highly abundant species were Porifera indet. 1, Buccinidae indet. *Bythocaris* sp. indet. and Amphipoda stet., which all had over 1700 recordings each. Eight morphospecies had less than 10 records in total, including the snailfish *Rhodichtys regina* and the ctenophore *Bathyctena* gen. inc. who were singletons.

Fauna was observed over the whole extent of the study area, with the exception of some areas around the active vents (Figure 3.2). Only nine of the morphospecies were present at all five study sites (all of the Cnidarian morphospecies, *Bythocaris* sp. indet., Buccinidae indet., Amphipoda stet. and *Lycenchelys platyrhina*). The Eastern periphery had the highest number of observations, almost twice as many as the Barite field, which had the second most observations. The Western mound had the lowest number of records, only 192 in total. There were no observations of the amphipods or small gastropods known to inhibit the black smoker chimneys, due to the distortion of the images collected over these steep areas, in addition to the very small size of these taxa (see Discussion).

3.1.1 Porifera

Four morphospecies of Porifera were found. The smallest morphospecies (Porifera indet. 1) was dominant with 1757 observations in total, while two other morphospecies were very rare (seven observations in total). A total of 12 occurrences of carnivorous sponges were also observed. Porifera indet. 2 was only found in the Barite field, while *Asconema megatriialia* and Cladorhizidae stet. were found in the Eastern and Western periphery. Porifera indet. 1 was found at all sites except the Barite field. At Loki West the sponges were concentrated in the south (see Appendix C). In general, they were not observed in areas of focused and diffuse venting.

3.1.2 Cnidaria

Three benthic and two mobile morphotypes of Cnidaria were found. All five morphospecies were recorded from all sites. Two of the Actiniaria morphospecies were very abundant, while Actiniaria stet. 3 was only observed 33 times. The actiniarians were generally not recorded close to the active vents (Appendix C). Actiniaria stet. 2 was mostly recorded from the periphery. The two jellyfish morphospecies did not seem to have a preference for venting or non-venting areas, as the observations were scattered. However, the jellyfish are highly mobile, so some caution needs to be taken in interpreting these patterns.

3.1.3 Ctenophora

There was only one observation of the ctenophore *Bathyctena* gen. inc. It was observed in the Barite field at Loki East.

3.1.4 Mollusca

Only one buccinid gastropod morphospecies was found. In total 1992 observations were made, and the majority of these were in the Barite field and the Eastern periphery. They were found at all five sites, and were scattered across most of the study area (Appendix C).

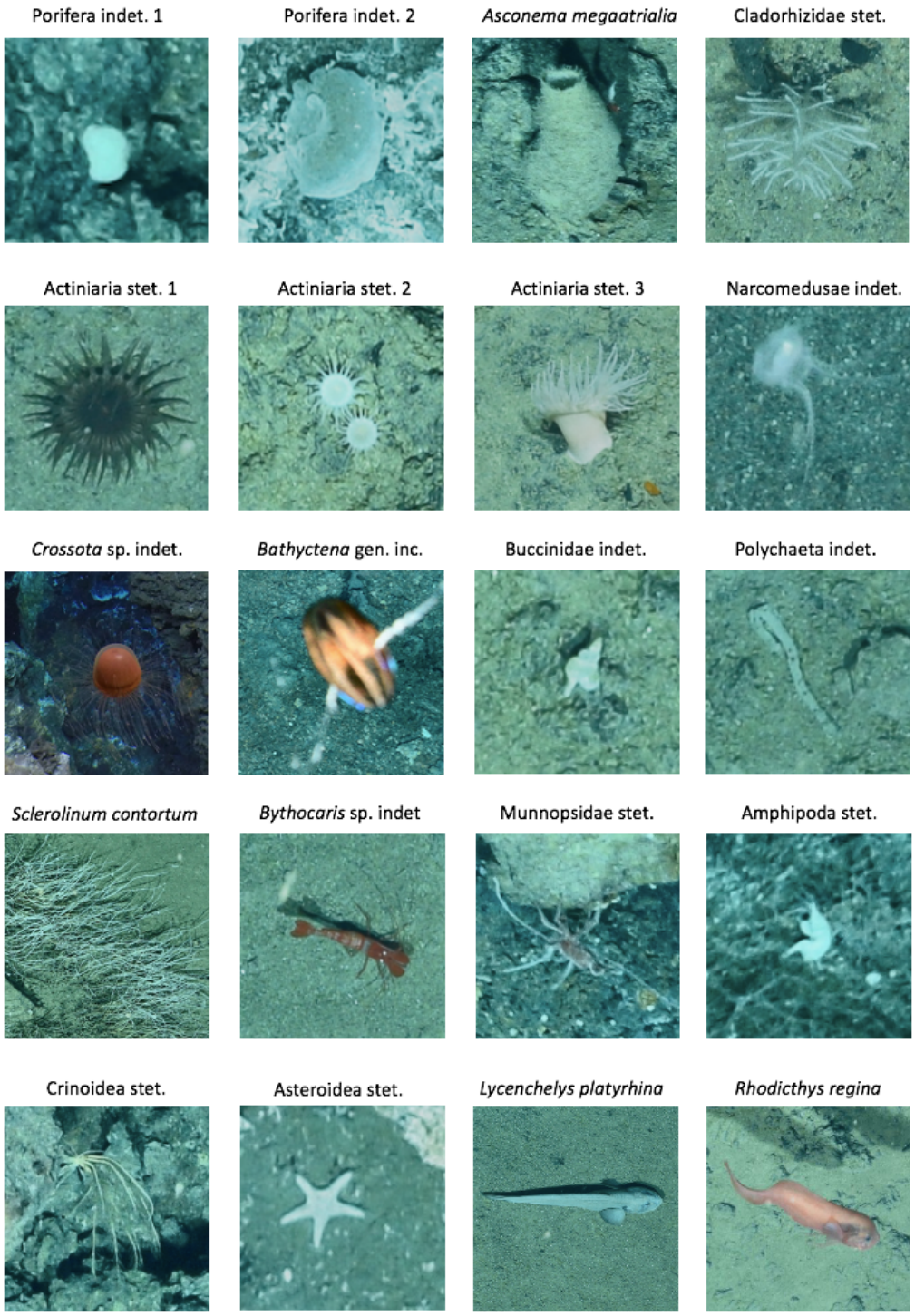

Figure 3.1: The 20 morphospecies observed from the photomosaics of Loki's Castle. The images are from the raw images that were used to compose the mosaics, except the image of *Crossata* sp. which is from a ROV closeup of better quality.

Table 3.1: Absolute abundance of each morphospecies at the five study sites at Loki's Castle in total number of individuals recorded. **Sclerolinum contortum* are quantified as proportional coverage.

Phylum	Morphospecies	Barite field	East mound	East periphery	West mound	West periphery	**Total**
Porifera	Porifera indet. 1	0	1	955	2	799	**1757**
	Porifera indet.2	3	0	0	0	0	**3**
	Asconema megaatrialia	0	0	2	0	2	**4**
	Cladorhizidae stet.	0	0	11	0	1	**12**
Cnidaria	Actiniaria stet. 1	404	202	1478	7	49	**2140**
	Actiniaria stet. 2	426	28	4379	1	101	**4935**
	Actiniaria stet. 3	1	9	16	2	5	**33**
	Narcomedusae indet.	6	1	14	4	3	**28**
	Crossata sp. indet.	12	6	46	8	13	**85**
Ctenophora	*Bathyctena* gen. Inc.	1	0	0	0	0	**1**
Mollusca	Buccinidae indet.	1178	76	672	20	45	**1991**
Annelida	Polychaeta indet.	1	0	1	0	0	**2**
	*Sclerolinum contortum**	0.24	0	0.006.	0	0	**-**
Arthropoda	*Bythocaris* sp. indet.	762	90	614	133	137	**1736**
	Munnopsidae stet.	4	2	11	0	0	**17**
	Amphipoda stet.	1675	7	70			**1752**
Echinodermata	Crinoidea stet.	3	0	3	4	1	**11**
	Asteroidea stet.	2	0	2	0	2	**6**
Chordata	*Lycenchelys platyrhina*	120	14	74	11	10	**229**
	Rhodicthys regina	0	0	1	0	0	**1**
	Total	**4598**	**436**	**8349**	**192**	**1168**	**14743**

3.1.5 Annelida

Of the two polychaete morphospecies, the majority were dense colonies of *S. contortum*. They occurred in the diffuse venting areas at Loki East and were not found at Loki West (Appendix C). There were only two observations of the second morphospecies, one in the Barite field and one in the Eastern periphery.

3.1.6 Arthropoda

Three morphospecies of arthropods were found, namely *Bythocaris* sp. indet., Amphipoda stet., and Munnopsidae stet. Both *Bythocaris* sp. indet. and Amphipoda stet. were abundant. *Bythocaris* sp. indet. was observed in most of the studied area, but was most abundant in

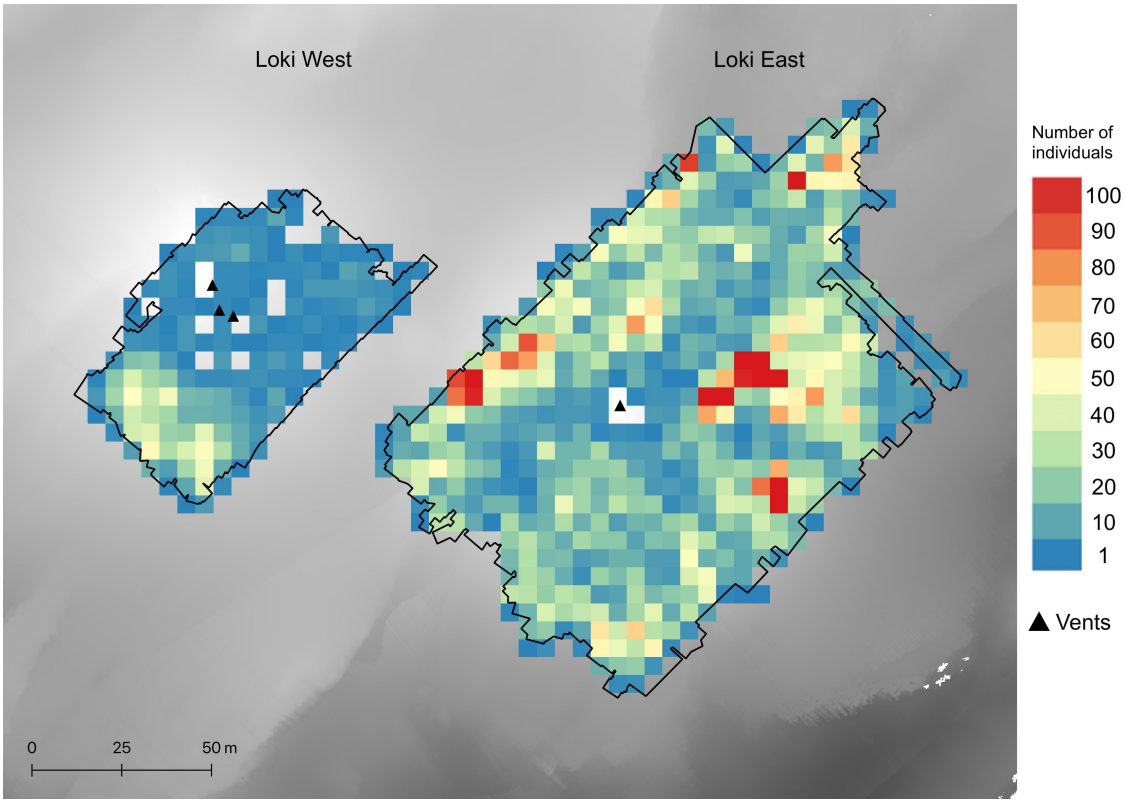

Figure 3.2: Spatial distribution of total faunal records from the photomosaics of Loki's Castle. Each pixel represents 5x5m. *S. contortum* is not included here as the data on this species were recorded as percentage coverage (but see Appendix C). Solid lines represent the photomosaic boundaries.

the Barite field and Eastern periphery (Appendix C). The vast majority of amphipods were recorded in the Barite field, but there were observations at all five sites. Munnopsid isopods occurred in low numbers and were not found in the Western mound or periphery.

3.1.7 Echinodermata

Echinoderms were not very abundant (17 observations in total). Two morphospecies were found, Crinoidea stet. and Asteroidea stet. Crinoidea stet. was not found in the Eastern mound, while Asteroidea stet. was not observed in the Eastern or Western mound. The observations were scattered, and they did not seem to have a preference for venting or non-venting areas (Appendix C).

3.1.8 Chordata

Two species of demersal fish were found. There was only one observation of the snailfish *R. regina*, in the Eastern periphery. The eelpout *L. platyrhina* was much more frequent, and was observed from all five sites. The observations of *L. platyrhina* were scattered, with a higher abundance in the Barite Field (Appendix C).

The pelagic and highly mobile fauna (i.e. Narcomedusae indet., *Crossota* sp. indet., *Bathyctena* gen. inc., and *R. regina*) were not included in further analysis. The reason is that their high mobility makes it very likely that the same individual is present in several pictures, and thereby counted several times throughout the photographic survey. The eelpout *L. platyrhina* was however included in the analysis, because they are benthic and associated with vents. Polychaeta indet., and Porifera indet. 2 were excluded from the further analysis due to the low number of observations (three or less observations).

3.2 Proportion of morphospecies

S. contortum was the dominant space-occupying species in the Barite field (0.24 mean percentage cover ± 0.02 SE). Based on square-root transformed densities, Buccinidae indet. (22%), Amphipoda stet. (20%) and *Bythocaris* sp. indet. (18%) also made up a large proportion of the fauna in the Barite field (Figure 3.3). In the Eastern mound the most prominent morphospecies were Actiniaria stet. 1 (31%), Bythocaris sp. indet. (26%) and Buccinidae indet. (23%). The Eastern periphery on the other hand was dominated by actiniarians. Actiniaria stet. 2 (38%) was most prominent, but Actiniaria stet. 1 was also abundant here (19%). The faunal community at the Eastern periphery was further characterized by abundant Bythocaris sp. indet. (13%), Buccinidae indet. (13%) and Porifera indet. 1 (11%).

Observations on the Western mound were dominated by *Bythocaris* sp. indet, which made up over 66% of the relative density of megafauna. Other prominent morphospecies at this site were *L. platyrhina* (13%) and Buccinidae indet. (9%). Faunal observations on the Western periphery were dominated by Porifera indet. 1 (45%), and there was also a relatively high proportion of *Bythocaris* sp. indet at this site (22%).

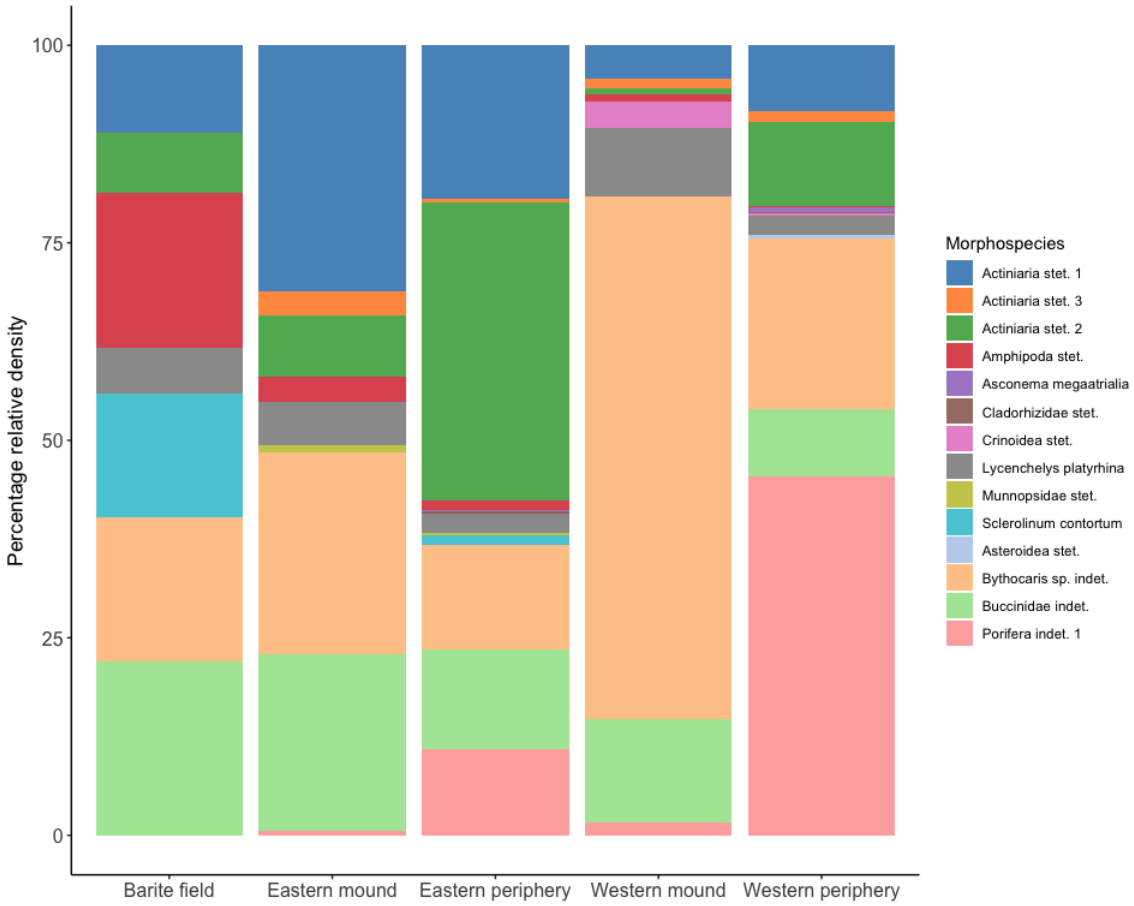

Figure 3.3: Proportion of morphospecies occurring in each study site, based on square root transformed densities, except for *S. contortum* which is based on square root transformed percentage coverage.

3.3 Density

The Barite field had the highest average square root transformed density (2.17 ± 0.08) of the five study sites (Figure 3.4). Then followed the Eastern periphery (1.26 ± 0.03), and the Eastern mound and Western periphery (1.01 ± 0.09 and 1.01 ± 0.07, respectively). The Western mound had the lowest average density (0.44 ± 0.03) and the lowest within-site spatial variation.

Amphipoda stet. occurred in high densities in the Barite field, and much lower densities at all other sites (Table 3.2). A similar pattern was seen for Buccinidae indet. and *Bythocaris* sp. indet. Actiniaria stet. 1 was found in highest densities at the Eastern mound, lower densities in the Barite field and Eastern periphery, and very low densities at the two Western sites.

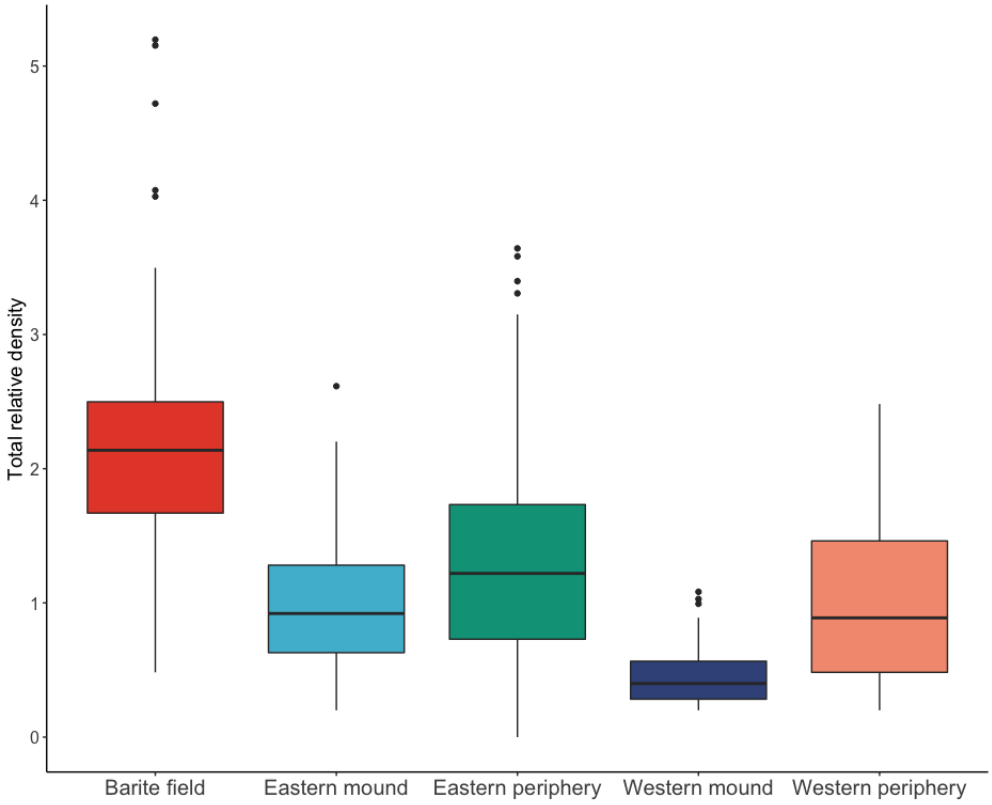

Figure 3.4: Total relative density of fauna at the five different study sites at Loki's Castle. Numbers are square root transformed. Horizontal lines are medians, boxes are upper and lower quartiles, vertical lines are upper and lower whiskers and dots are outliers.

Actiniaria stet. 2 had the highest density in the Eastern periphery, followed by the Barite field. At the three other sites it was found in low densities. The density of Porifera indet. 1 was highest in the Western periphery, and low at all other sites. Compared to Porifera indet. 1, other morphospecies had a very low density in the Western periphery. The Western mound was characterized by low densities of all morphospecies found there.

The hexactinellid *A. megaatrialia*, Cladorhizidae stet., Actiniaria stet. 3, Munnopsidae stet., Crinoidea stet., Asteroidea stet., and *L. platyrhina* only occurred in low densities. The coverage of *S. contortum* per m^2 was low in the Eastern periphery and much higher in the Barite field. It was not found at the other sites.

Table 3.2: Average densities (ind. m^{-2}) and standard error for the most common morphospecies at the five different study sites at Loki's Castle. *Numbers for *Sclerolinum contortum* are average percentage coverage and standard error.

Morphospecies	Barite field	Eastern mound	Eastern periphery	Western mound	Western periphery
Porifera indet. 1	0	0.001 (± 0.001)	0.08 (± 0.01)	0.001 (± 0.001)	0.41 (± 0.06)
Asconema megaatrialia	0	0	0.0002 (± 0.0001)	0	0.001 (± 0.0007)
Cladorhizidae stet.	0	0	0.001 (± 0.0005)	0	0.0005 (± 0.0005)
Actiniaria stet. 1	0.14 (± 0.02)	0.21 (± 0.05)	0.13 (± 0.01)	0.005 (± 0.003)	0.03 (± 0.005)
Actiniaria stet. 2	0.15 (± 0.04)	0.03 (± 0.01)	0.39 (± 0.02)	0.0007 (± 0.0007)	0.05 (± 0.01)
Actiniaria stet. 3	0.0004 (± 0.0004)	0.009 (± 0.005)	0.001 (± 0.0004)	0.002 (± 0.001)	0.003 (± 0.001)
Buccinidae indet.	0.41 (± 0.03)	0.08 (± 0.01)	0.06 (± 0.005)	0.02 (± 0.004)	0.02 (± 0.005)
*Sclerolinum contortum**	0.24 (± 0.02)	0	0.006 (± 0.002)	0	0
Bythocaris sp. indet.	0.27 (± 0.02)	0.09 (± 0.01)	0.05 (± 0.003)	0.1 (± 0.009)	0.07 (± 0.008)
Munnopsidae stet.	0.001 (± 0.0007)	0.002 (± 0.001)	0.001 (± 0.0003)	0	0
Amphipoda stet.	0.59 (± 0.12)	0.007 (± 0.003)	0.006 (± 0.002)	0.0007 (± 0.0007)	0.0005 (± 0.0005)
Crinoidea stet.	0.001 (± 0.0006)	0	0.0003 (± 0.0002)	0.003 (± 0.001)	0.0005 (± 0.0005)
Asteroidea stet.	0.0007 (± 0.0005)	0	0.0002 (± 0.0001)	0	0.001 (± 0.0007)
Lycenchelys platyrhina	0.04 (± 0.005)	0.01 (± 0.005)	0.007 (± 0.0008)	0.008 (± 0.003)	0.005 (± 0.002)

3.4 Diversity indices

The Eastern periphery had the highest amount of morphospecies, while the two mounds had the lowest morphospecies richness (Table 3.3). The Kruskal-Wallis test showed that there were significant differences between sites in Shannon diversity index ($p < 0.001$), Simpson diversity index ($p < 0.001$) and Pielou's evenness ($p < 0.001$). In general, the diversity indices were lower for the sites at Loki West and higher for the Eastern sites.

The Barite field had the highest Shannon diversity index and Simpson diversity (Dunn test; $p < 0.001$). Then followed the Eastern mound and Eastern periphery. There was a significant difference between these two sites for the Shannon index (Dunn test; $p = 0.03$), but not for the Simpson index (Dunn test; $p = 0.16$). For Pielou's evenness the Barite field and the Eastern mound had the highest values, but there was no significant difference between these two sites (Dunn test; $p = 0.25$). They did however have higher evenness values than the Eastern periphery (Dunn test; $p < 0.001$).

Table 3.3: Average (± SE) diversity indices for areas of Loki's Castle: number of morphospecies present (S), Shannon diversity index(H), Simpson diversity index (1-D) and Pielou's evenness (J).

	S	H	1-D	J
Loki East				
Barite field	11	1.22 (± 0.03)	0.64 (± 0.01)	0.75 (± 0.01)
Mound	9	0.81 (± 0.07)	0.51 (± 0.04)	0.71 (± 0.05)
Periphery	14	0.65 (± 0.02)	0.48 (± 0.01)	0.56 (± 0.02)
Total	14	0.76 (± 0.02)	0.51 (± 0.01)	0.60 (± 0.01)
Loki West				
Mound	9	0.29 (± 0.05)	0.34 (± 0.05)	0.35 (± 0.06)
Periphery	12	0.54 (± 0.05)	0.33 (± 0.03)	0.49 (± 0.04)
Total	12	0.43 (± 0.04)	0.34 (± 0.03)	0.43 (± 0.03)

There was no significant difference between the Western mound and Western periphery in Pielou's evenness or Simpson diversity index (Dunn test; $p = 0.16$ and $p = 0.34$, respectively). They were however lower than the sites at Loki East (Dunn test; $p < 0.01$). The Western mound had the lowest Shannon diversity index of all sites (Dunn test; $p < 0.001$).

3.5 Morphospecies assemblages

The two sites at Loki West clearly differed from each other, and there was no overlap in the 50% confidence ellipses between these two sites (Figure 3.5). The three sites at Loki East had distinct but somewhat overlapping confidence ellipses. There was especially overlap between the Barite field and the Eastern mound, but there was also a bit of overlap between the Eastern periphery and the Barite field. The PERMANOVA analysis showed that the groups made by the nMDS explained 25% of the variation in dissimilarity between sites ($p = 0.001$).

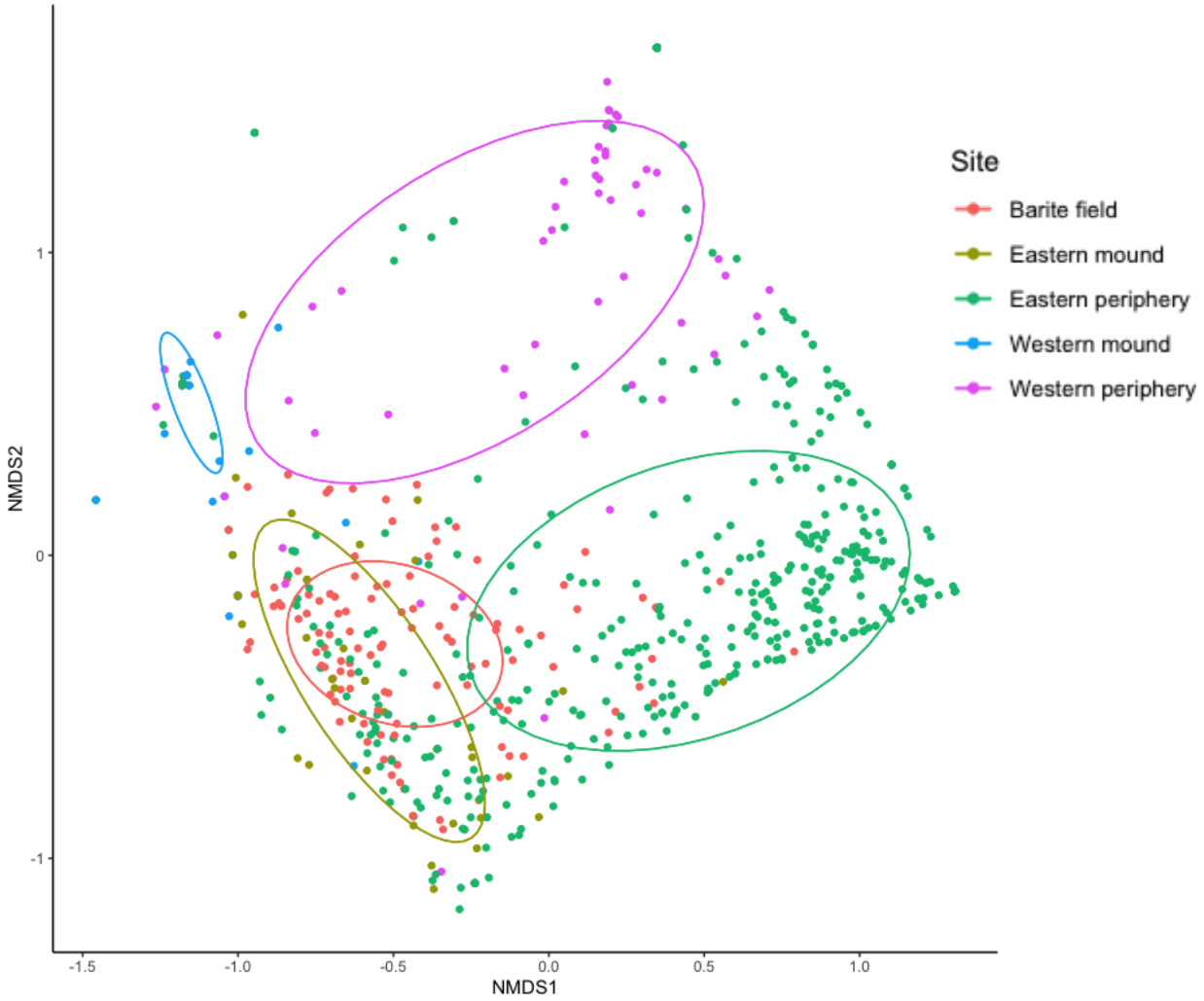

Figure 3.5: Non-metric Multidimensional Scaling (nMDS) plot of morphospecies assemblage at the five study sites at Loki's Castle using a Bray-Curtis dissimilarity matrix. Each point represents one 5x5m grid cell and the ellipses are 50% confidence ellipses. Stress value = 0.14.

The results from the pairwise Adonis analysis showed that the largest dissimilarity in morphospecies assemblage was between the Barite field and the Western mound (37%, p = 0.001). According to the SIMPER analysis, *Bythocaris* sp. indet., *S. contortum* and Buccinidae indet. were the three species contributing the most to this difference (Table 3.4). There was 30% dissimilarity between the Barite field and the Western periphery (p = 0.001). *S. contortum*, Porifera indet. 1 and *Bythocaris* sp. indet. contributed the most to the dissimilarity between these two sites.

Table 3.4: Results from the pairwise PERMANOVA and SIMPER analyses.

PERMANOVA			SIMPER (% contribution)		
Sites	R2	P-value	#1	#2	#3
East periphery vs Barite field	0.17	0.001	Actiniaria stet. 2 (17.5%)	*S. contortum* (14.8%)	*Bythocaris* sp.indet (13.6%)
East periphery vs West periphery	0.07	0.001	*Bythocaris* sp. indet (20.3%)	Actiniaria stet. 2 (19.6%)	Porifera indet. 1 (17%)
East periphery vs West mound	0.14	0.001	*Bythocaris* sp. indet. (27.3%)	Actiniaria stet. 2 (20.7%)	Actiniaria stet. 1 (11%)
East periphery vs East mound	0.05	0.001	Actiniaria stet.. 2 (20%)	*Bythocaris* sp. indet (19.5%)	Actiniaria stet. 1 (14.5%)
Barite field vs West periphery	0.30	0.001	*S. contortum* (15.8%)	Porifera indet. 1 (14.7%)	*Bythocaris* sp. indet. (14.3%)
Barite field vs West mound	0.37	0.001	*Bythocaris* sp. indet. (19%)	*S. contortum* (18.4%)	Buccinidae indet. (16.7%)
Barite field vs East mound	0.16	0.001	*S. contortum* (19.2%)	*L. platyrhina* (14.7%)	*Bythocaris* sp. indet. (14%)
West periphery vs West mound	0.18	0.001	*Bythocaris* sp. indet. (26.8%)	Porifera indet. 1 (21.4%)	Buccinidae indet. (10.3%)
West periphery vs East mound	0.12	0.001	*Bythocaris* sp. indet. (20%)	Porifera indet. 1 (17.9%)	Actiniaria stet. 1 (15.4%)
West mound vs East mound	0.19	0.001	*Bythocaris* sp. indet (24.7%)	Actiniaria stet. 1 (18.8%)	Buccinidae indet. (18.6%)

The Eastern periphery and Eastern mound were the two most similar sites (R2 = 0.05, p = 0.001). The analysis also showed a large degree of similarity between the Eastern periphery and Western periphery (R2 = 0.07, p = 0.001). The morphospecies assemblage at the Barite field was 17% dissimilar to the Eastern periphery and 16% dissimilar to the Eastern mound. The dissimilarity between the Western mound and Western periphery was 18%, and this was mostly influenced by *Bythocaris* sp. indet., Porifera indet. 1 and Buccinidae indet. Overall, *Bythocaris* sp. indet. was the species that contributed most to the difference between sites.

3.6 Spearman's Rank Correlations

3.6.1 Correlations with abiotic factors

Heat flux and temperature were negatively correlated with both actiniarian morphospecies and Porifera indet. 1, and positively correlated with the other morphospecies (Table 3.5). Roughness and slope were negatively correlated with Amphipoda stet., *Bythocaris* sp. indet., Buccinidae indet., and *S. contortum*. Roughness was positively correlated with both Actiniarian morphospecies, while slope was also positively correlated with Porifera indet.1, in addition to the Actiniarians. Northness had a slight positive correlation with Amphipoda stet., and a slight negative correlation with Actiniaria stet. 2. Eastness was not significantly correlated with any of the morphospecies.

Table 3.5: Spearman's rank correlations of abiotic factors and the most common morphospecies at Loki's Castle. Significant correlations ($p < 0.05$) are highlighted in green.

Abiotic factors						Morphospecies							
	Temperature	Roughness	Slope	Northness	Eastness	Actiniaria stet. 1	Actiniaria stet. 2	Amphipoda stet. 3	*Lycenchelys platyrhina*	Bythocaris sp. indet.	Buccinidae indet.	Porifera indet. 1	*Sclerolinum contortum*
Heat flux	1	-0.16	-0.16	-0.04	-0.03	0.01	-0.35	0.57	0.34	0.50	0.37	-0.34	0.61
Temperature		-0.16	-0.16	-0.04	-0.04	0.02	-0.35	0.58	0.36	0.50	0.38	-0.34	0.63
Roughness			0.97	-0.05	-0.01	0.04	0.07	-0.19	-0.13	-0.14	-0.07	-0.02	-0.18
Slope				-0.05	-0.01	0.02	0.04	-0.2	-0.14	-0.18	-0.08	-0.05	-0.19
Northness					0.03	-0.02	-0.03	-0.03	-0.03	0.02	-0.06	-0.01	-0.03
Eastness						0.05	0.05	0.02	0.03	0.03	0.04	-0.04	0.05
						Actiniaria stet. 1	0.22	0.22	0.13	0.28	0.37	-0.19	0.19
							Actiniaria stet. 2	-0.15	-0.02	-0.15	0.09	0.33	-0.11
								Amphipoda stet.	0.46	0.48	0.52	-0.21	0.75
									Lycenchelys platyrhina	0.33	0.30	-0.13	0.44
										Bythocaris sp. indet.	0.44	-0.22	0.50
											Buccinidae indet.	-0.17	0.59
												Porifera indet. 1	-0.23

3.6.2 Correlations between morphospecies

There was a strong positive correlation between *S. contortum* and Amphipoda stet. (Table 3.5). *S. contortum* also showed a strong positive correlation with Buccinidae indet., *Bythocaris* sp. indet. and *L. platyrhina*, and a slight positive correlation with Actiniaria stet. 1. Porifera indet. 1 and Actiniaria stet. 2 was negatively correlated with *S. contortum*. Porifera indet. 1 was negatively correlated with all morphospecies except Actiniaria stet. 2, where there was a positive correlation. Amphipoda stet., *L. platyrhina*, *Bythocaris* sp. indet. and Buccinidae indet. all were all positively correlated with each other.

3.7 Influence of environmental parameters

The results of the GAM analysis showed that temperature and slope were significant for both the total abundance and the species richness (Table 3.6). However, the model explained relatively little of the variation, only 16.9% and 17.1% respectively. Of the morphospecies tested, the model best explained the variance in *S. contortum* (58.8%). For the rest of the

morphospecies, temperature and slope explained less than 50% of the variation. The model was in particular not a good fit for three morphospecies where it explained less than 6% of the variation: Porifera indet. 1, and Actiniaria stet. 1 and 2 (see Appendix D for the model smoothing curves).

Table 3.6: Results from the GAM analysis. P-value of the abiotic factors included in the model, and the deviance explained by the model. Both abiotic factors contained a smoothing function.

Response	Temperature	Slope	Deviance explained
Total abundance (N)	<0.001 ***	<0.001 ***	16.4%
Species richness (S)	<0.001 ***	<0.001 ***	17.1%
Porifera indet. 1	0.005 **	0.013 *	2.4%
Actiniaria stet. 1	0.729	0.270	0.2%
Actiniaria stet. 2	<0.001 ***	<0.001 ***	5.2%
Buccinidae indet.	<0.001 ***	0.014 *	26.2%
Sclerolinum contortum	<0.001 ***	0.015 *	58.8%
Bythocaris sp. indet.	<0.001 ***	<0.001 ***	37.5%
Amphipoda stet.	<0.001 ***	0.017 *	19.8%
Lycenchelys platyrhina	<0.001 ***	0.224	28.1%

4. Discussion

4.1 Limitations

My thesis provides, for the first time, a spatial characterization of the benthic megafauna community inhabiting Loki's Castle vent field. Despite the complete visual coverage of the two mounds and surrounding areas through the photomosaics, there were a few limitations associated with this method, and image analysis in general. One limiting factor of image analysis is that for some species the identifying morphological characteristics cannot be seen in images, and they can therefore not be identified to species level from photos only. For example, there are several amphipod species at Loki's Castle (Tandberg *et al.*, 2012, 2018), but from the images it was not possible to distinguish between them. The 20 morphospecies described in this thesis is therefore an underestimate of the true megafaunal diversity, as some of them probably are different species with similar morphology. In addition, the fauna living inside *S. contortum* colonies could not be observed from the photos, and several species that are known to inhabit these colonies are therefore not included in this study (Kongsrud & Rapp, 2012; Kongsrud *et al.*, 2017). The same caveat applies to fauna inhabiting other cryptic habitats, such as inside sponges. Image analysis also does not allow for observations of meiofauna or infauna, which is why this thesis focuses on the megafauna.

The gastropods *Pseudosetia griegi* and *Skenea* spp., as well as amphipods such as *Exitomelita sigynae*, are known to populate the chimney walls at Loki's Castle (Pedersen *et al.*, 2010; Tandberg *et al.*, 2012), but this could not be observed in this study. They could not be visualized from the mosaic due to the greater distortion in the images taken in the steeper part of the mounds around the active vents. Since the images only are taken from above it is not possible to fully observe the complex 3D-structure of the vents, and the images directly above vents were also disturbed by the hydrothermal plume in many cases. In addition, the small size of these species makes it difficult to detect them from images with this pixel resolution. A few individuals of amphipods were recorded from the vents, but they are likely more abundant in this area.

Overlapping photos also pose a problem with image analysis. Topographic features were used to compare photos and minimized double counts, but a small degree of double counting is still expected, especially for mobile morphospecies such as *Bythocaris* sp. indet. and *L. platyrhina*. Mobile species can move their position in the time between two photos are taken, which makes it difficult to confirm if they are the same individual.

4.2 Differences between study sites

There were statistically significant differences between the five study sites in density, diversity and composition of morphospecies. This indicates that Loki's Castle vent site is a highly heterogenous site, with venting structures creating a range of habitats within a gradient of abiotic factors. There were clear differences in the composition of morphospecies occupying each study site, and even the two peripheral sites differed from each other (Figure 4.1). Typically, one or a few morphospecies dominated at each site, while the other morphospecies were found at low densities. Although the density and composition differed, most of the morphospecies were found at several sites, so the communities seem to be closely connected, which is expected given the small spatial scale of the survey, and the fact that the most surveyed species are not strictly associated with active venting habitats.

4.2.1 Barite field

The Barite field had the most diverse and dense fauna of the five study sites. While the Eastern mound and periphery had one or two dominating morphospecies, six different morphospecies were found at relatively high densities in the Barite field. This is reflected in the biodiversity indices, all diversity indices except for the number of morphospecies (S) were highest in the Barite field. Diffuse venting areas have less extreme conditions than the focused vents, making it possible that more species are able to tolerate these conditions. The highest biomass of metazoans are thus often found in areas of diffuse venting (Fisher *et al.*, 2007). The average temperatures in the Barite field ranged between 0°C and 13°C above the ambient seawater, which is -0.7°C. For comparison, the grid cell containing the João chimney had an average temperature of 53°C. Habitats of intermediate stress have shown to host the highest richness of macrofauna at hydrothermal vents, and it is hypothesized that adaptations make macrofaunal vent species able to take advantage of the high food availability at these sites while maintaining physiological homeostasis (Gollner *et al.*, 2015).

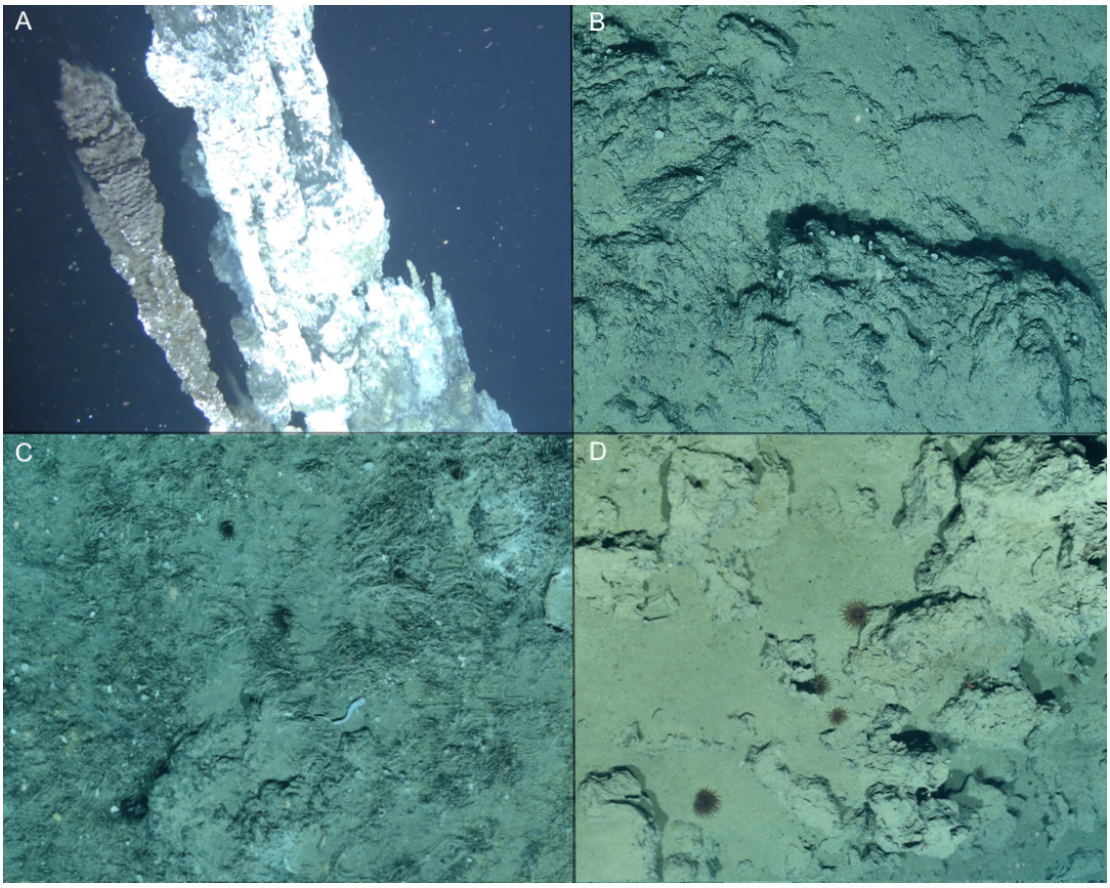

Figure 4.1: A) An active chimney with white bacterial mats. **B)** The Western periphery dominated by Porifera indet. 1. **C)** The Barite field with *S. contortum*, *L. platyrhina*, Actiniaria stet. 1, Actiniaria stet. 2., Amphipoda indet. and Buccinidae indet. **D)** The Eastern periphery with Actiniaria indet. 1.

The nature of the diffuse venting through cracks in the seafloor creates large temperature variations on very small scales in the Barite field (T. Barreyre, personal communication). Microhabitats created by these kind of heterogeneous conditions provides niches for specialized animals, which could enhance diversity (McClain & Schlacher, 2015). Mobile fauna responds quickly to fluctuating temperatures and move to temperatures well within their thermal tolerance range, while sessile species depend on selecting a microhabitat with tolerable temperatures (Bates *et al.*, 2010). The existence of different microhabitats within the Barite field might also explain why some grid cells have very high faunal densities. In addition, colonies of *S. contortum* have a facilitating role in the benthic community by providing important habitat for many species (Decker *et al.*, 2012; Kongsrud & Rapp, 2012; Tandberg *et al.*, 2018). Although the infauna known to occur within the *S. contortum* colonies could not be recorded from the photomosaic, it probably accounts for an indirect positive effect in

the benthic community at the Barite field, where the high abundance of prey attracts more predators, such as fish, shrimp or buccinid gastropods.

4.2.2 Mounds

Both mounds had a lower total density than the surrounding periphery, however this excludes snail and amphipod species known to occur in high densities on active chimneys (see section 4.1 – Limitations). While the Eastern mound was more diverse than the periphery, the Western mound had diversity indices that were lower or similar to the Western periphery. The high abundance of Actiniaria stet. 1 at the Eastern mound was the most striking difference in morphospecies composition between the two mounds, but according to the SIMPER analysis *Bythocaris* sp. indet. and Buccinidae indet. also contributed to this difference. It is possible that the higher density of actiniarians and buccinid gastropods at the Eastern mound is due to enhanced food availability at this site because of its proximity to the Barite field. The Western mound had few observations and most of them were of *Bythocaris* sp. indet. This area does have abundant bacterial mats, and the lack of observations could indicate that the abiotic conditions here are too harsh for many species.

It is not surprising that a lower number of morphospecies were recorded at the mounds compared to the other sites. Diversity and abundance of macrofauna generally decline towards the highest hydrothermal activity (Gollner *et al.*, 2015; Bell *et al.*, 2016). The vent fluid emerging from the hydrothermal vents at Loki's Castle have a temperature of 310-320°C and high concentrations of dissolved metals (Pedersen *et al.*, 2010). Hydrothermal vent macrofauna are not able to tolerate temperatures over 60°C (Lee, 2003), so the conditions close to the active black smokers are uninhabitable for most organisms other than chemosynthetic bacteria. There were in general very few observations from the grid cells with the highest average temperatures, but as earlier mentioned one of the limitations of this study is that fauna on the active chimneys could not be detected in the photomosaic.

4.2.3 Peripheral areas

The peripheral areas could be statistically separated from the hydrothermal active areas, even though they host many of the same species. The two peripheral sites mostly lacked typical vent-endemic taxa such as *S. contortum* and vent-associated amphipods, but had a high

density of certain background taxa, such as actiniarians and sponges. This is characteristic of peripheral vent communities that act as intermediate zones between the specialized community around vents and the regular deep-sea community (Sen *et al.*, 2016). The density of background species is often much higher in the peripheral zone than in the surrounding deep sea, probably due to the enhanced local food supply around vents (Arquit, 1990; Sen *et al.*, 2016). Because of this, the total density of peripheral zones can be close to the density of the hydrothermal active zones.

The highest number of morphospecies was found at the peripheral sites. Being transition zones between vent-specific communities and background communities, peripheral areas are often inhabited by species from both of these sites (Sen *et al.*, 2016). Peripheral areas are less influenced by the extreme conditions of hydrothermal vents, which could mean that more species are able to inhabit this area. Although having the highest number of morphospecies, the two peripheral sites were dominated by one or two morphospecies, while the other morphospecies present were mostly found in small densities.

4.3 Community differences between East and West

A general pattern was that the megafaunal communities at the Eastern sites were denser and more diverse than the communities at the Western sites, both for the mounds and the peripheries. For the peripheral sites there was also a clear difference in the most abundant morphospecies – actiniarians dominated the Eastern site while the Western site was characterized by a high abundance of sponges. It is possible that the higher density and diversity of the East is connected to its proximity to the Barite field, and that the high productivity from the diffuse venting site have extended benefits to the nearby communities. This hypothesis seems to be supported by the nMDS analysis where the confidence ellipses of the Eastern sites are partly overlapping, indicating a certain degree of similarity, or a transitioning in community composition between sites, suggesting the presence of an environmental gradient.

Kim & Hammerstrom (2012) proposed that the predominant flow direction from vents influenced the difference seen between southern and northern areas of the periphery at Lau Basin, where downcurrent sites had higher diversity. At Loki's Castle, the bottom current across the vents flow mostly in the Southeast direction, which might explain the higher

density and diversity seen in the East (Figure 4.2). Further strengthening this hypothesis is the fact that the fauna observed at the Western sites are mostly typical background taxa,

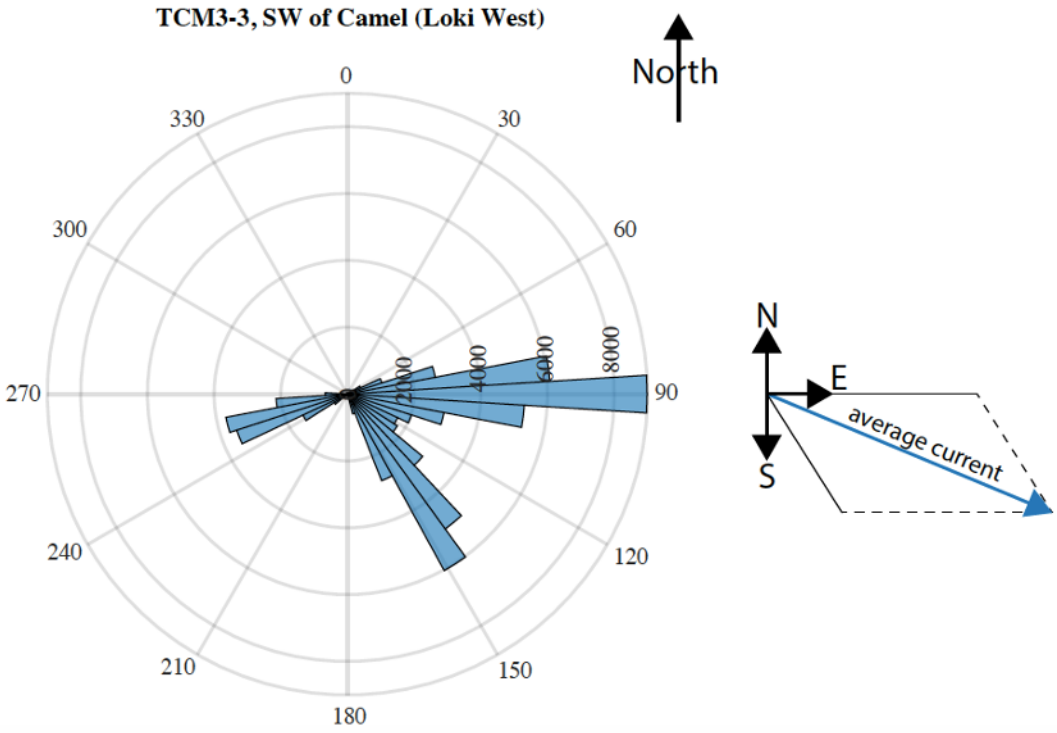

Figure 4.2: The predominant bottom current direction pattern measured from the active vent Camel at Loki's Castle. Courtesy of Dr. Thibaut Barreyre, Department of Earth Sciences of the University of Bergen.

such as sponges and shrimp. In addition to hydrothermal fluid flow, differences in substrate could contribute to faunal differences between peripheral areas (Podowski *et al.*, 2010; Kim & Hammerstrom, 2012; Sen *et al.*, 2016). Observations from images indicate that the Western periphery has a higher predominance of non-hydrothermal hard substrate, but this has not been quantified.

4.4 Distribution patterns of the most prominent morphospecies

Porifera indet. 1. The highest concentration of Porifera was in the south of the Western periphery. At the Eastern site, the sponges were mostly observed at the edge towards Loki

West, which makes it likely that the aggregations observed at these two sites are connected. However, there were no ROV images available for the area between the two mosaics to confirm this. The availability of hard substrate and increased amount of suspended food particles probably benefit sponges in the peripheral areas around hydrothermal activity (Georgieva *et al.*, 2020). Although substrate was not recorded in detail for this study due to time restrictions, a general overview of the images indicates a higher occurrence of basaltic outcrops in the area where the sponges aggregated. The observation of basaltic outcrops was also validated from ROV video footage from other dives.

The bottom current pattern might also affect sponge settlement. The water current from the active vents at Loki's Castle flows mostly in the Southeast direction, and the distribution map of Porifera indet. 1 shows that the sponges at Loki's Castle in general were not recorded from the areas that would be directly affected by vent fluid (Appendix C). This could indicate that the sponges are sensitive to the chemical concentration of the vent plume. There were also no sponges observed in the Barite field. In addition to sponges avoiding vent fluids, a reason for this could be that there is simply no suitable substrate for the sponges to settle on, as the Barite field consists mostly of soft bottom and have a high coverage of *S. contortum*.

Actiniarians. Actiniarians dominated the Eastern periphery but were not very abundant in the Western periphery. There could be several explanations for why they are mostly present at the Eastern site. One reason could be that the substrate is different at the two sites, and that the Eastern site has a substrate that favors actiniarians, for example substrate with smoother surfaces (Podowski *et al.*, 2010). A different explanation could be that the Eastern periphery has a higher food availability from suspended organic matter. Deep sea anemones usually feed by suspension feeding or prey capture, but there have also been reports of actiniarians living in symbiosis with chemotrophic bacteria in the Gulf of California (Goffredi *et al.*, 2021). An important food source for actiniarians in the peripheral zone might be patches of bacteria that have broken off the substrate (Galkin, 1997). There were a few observations where individuals of Actiniaria stet. 1 seemed to be feeding on detached bacterial patches (Figure 4.3).

There was a clear difference in distribution of the two most abundant actiniarian morphospecies. Actiniaria stet. 1 was observed closer to active vents, and also occupied more of the Barite field than the smaller sized Actiniaria stet. 2. It can therefore seem like the first morphospecies have a higher tolerance for the variable conditions created by the vent plume than the other

morphospecies. Interestingly, Actiniaria stet. 2 is present in the Northern part of the Barite field (sometimes referred to as the Oasis), but not in the rest of the Barite field. The reason for this is unclear, as the areas seem to be quite similar in temperature and heat flux. There could

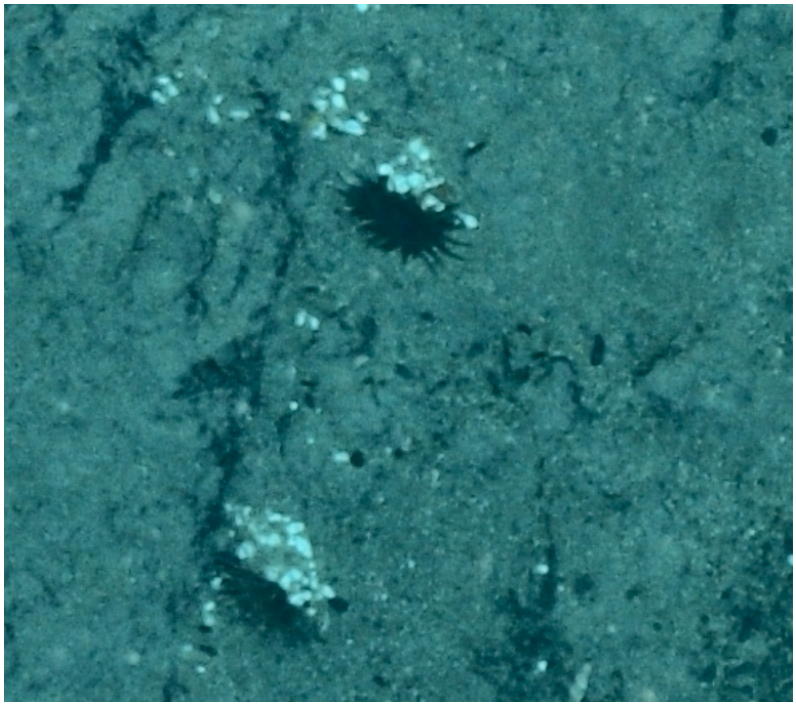

Figure 4.3: Actiniaria stet. 1 seemingly feeding on detached bacterial patches.

however be small-scale differences that cannot be observed from the 5x5m grid, or differences in substrate. Observations indicate that Actiniaria stet. 1 settles on sedimented areas, while Actiniaria stet. 2 settles on bare rock. In general, Actiniaria stet. 1 was less abundant in the edges of the mosaic, where Actiniaria stet. 2 were dominating.

Sclerolinum contortum. The tubeworm *S. contortum* was almost exclusively found in the diffuse venting area known as the Barite field. In the few cases where it was found in the Eastern periphery it was right on the edges of the Barite field. This species does not have a mouth or gut and therefore relies on the symbiosis with chemosynthetic bacteria (Lösekann *et al.*, 2008), which means that it is unable to survive in areas with too low hydrogen sulphide concentrations to feed their symbionts. Because this species is able to quickly colonize sulphur rich habitats and spread over large distances, it has been called a "chemosynthetic weed"

(Georgieva *et al.*, 2015), and in the Barite field some grid cells had up to 80% coverage by *S. contortum* colonies.

Amphipoda stet. Amphipods were mostly found on *S. contortum* colonies in the Barite field, but there were also a few recordings from the other sites. Grazing of chemosynthetic bacteria is probably the most important food source for amphipods at Loki's Castle (Tandberg *et al.*, 2012, 2018), and their distribution could be due to the high presence of bacterial mats in the Barite field. It is however striking that amphipods were completely absent from the Northern area of Loki West, an area also characterized by abundant bacterial mats. This suggests that the habitat provided by *S. contortum* is important for the presence of amphipods, although positive interactions with other species cannot be discarded. We know that amphipods are also found at the active chimneys (see section 4.1 - Limitations), so their density at the Eastern and Western mound are likely underestimated in this thesis.

***Bythocaris* sp. indet.** *Bythocaris* shrimp were found all over the study area, but interestingly their density was higher in the Barite field than at the other sites. The reason for the higher density of *Bythocaris* shrimp at the Barite field is not entirely clear. One plausible explanation could be that there is a cascading positive effect where a high density of prey facilitated by *S. contortum* colonies leads to a higher density of *Bythocaris* shrimp. They seem to tolerate variable abiotic conditions, as they were observed both close to active vents and in peripheral areas. However, it is worth noting that they are mobile and can easily move between different areas, meaning that they do not necessarily have to withstand the extreme conditions for a long period of time.

Buccinidae indet. The density of buccinid gastropods was much higher in the Barite field than at the other sites, even though they were present at all study sites. Some gastropod species have been shown to actively seek habitats with warm venting fluids, but avoid temperatures over a certain limit (Bates *et al.*, 2005). If there is high competition for food or space, some individuals may have to occupy habitats outside their preferred conditions (Bates *et al.*, 2005). The buccinid gastropods were least abundant in the Western periphery and mound. Deep-sea buccinids are predators and scavengers (Aguzzi *et al.*, 2012), and it is highly likely that higher food availability at the Eastern side attract more individuals.

Lycenchelys platyrhina. The eelpout *L. platyrhina* was distributed over the whole study area, but occurred at a higher density in the Barite field. Other species of eelpout at hydrothermal vents have been shown to feed on gastropods, amphipods and some polychaetes

(Sancho *et al.*, 2005). It is likely that *L. platyrhina* is more abundant in the Barite field because this site has a higher abundance of the benthic species that they prey on. This species is known from the Jan Mayen area and the Fram Strait, where only a few individuals have been recorded (Wienerroither *et al.*, 2011; Mecklenburg *et al.*, 2018). Compared to this, the abundance at Loki's Castle seems to be unusually high.

4.5 Abiotic factors

The extreme and variable abiotic conditions at hydrothermal vents, such as temperature and chemical exposure, are expected to be the most important structuring factors of the faunal community (Micheli *et al.*, 2002). Of the abiotic factors included in this study, temperature was by far the most influential on morphospecies distribution. Species have different tolerance levels to the variable temperatures at hydrothermal vents (Lee, 2003), which could explain some of the difference in spatial distribution between species. However, temperatures at vents covaries with the presence of vent fluids that contain sulfide and heavy metals, which depending on adaptations could be either toxic or beneficial to a species (McMullin *et al.*, 2007).

Several morphospecies were clearly associated with increased water temperatures. This was in particular *S. contortum* and amphipods, but also *L. platyrhina*, *Bythocaris* shrimp and Buccinidae indet. were positively correlated with warmer temperatures. The difference in abundance and species richness between sites could partly be explained by differences in temperature and slope, but most of the difference could not be explained by any of the tested variables. Since there are often large variations in temperature over short time at hydrothermal vents, these variations might be more important than the average temperature animals are exposed to (Johnson *et al.*, 1988). The temperature measurements had a limited time span, and may thus not have captured the entire range of abiotic variation and species responses to such changes.

Temperature could explain most of the distributional patterns of *S. contortum*. Since this species also inhabits cold seeps and organic falls (Eilertsen *et al.*, 2018), temperature itself is probably not determining their distribution, but rather one or more co-varying parameters, such as the sulphide concentration and the presence of chemosynthetic bacteria that are associated with higher temperature areas at Loki's Castle. For most of the other morphospecies it was clear that temperature is an important structuring factor, but that there are also other

factors influencing where they are found. This could be other abiotic factors not studied in this thesis, such as substrate and chemical components of the vent fluids (Sarrazin *et al.*, 1999), or biological interactions such as competition and predation (Micheli *et al.*, 2002; Levesque *et al.*, 2003). Even though amphipods were clearly correlated with temperature, most of its distribution was explained by other unknown factors. Porifera indet. 1 and Actiniaria stet. 2 were clearly associated with background temperatures. Actiniaria stet. 1 was the morphospecies least influenced by temperature, and temperature and slope could not explain the distribution of this species at all. This reflects the fact that this morphospecies were found both in the warm areas close to active vents, and in cold background areas.

Although slope and roughness were significantly correlated with the abundance of most of the morphospecies, their influence on morphospecies distributions were minor compared to temperature. At hydrothermal vents, the steep gradients of temperature and chemicals from vent fluids might make other abiotic factors become less important. Some morphospecies were negatively correlated with slope and roughness, while others were positively correlated. This could reflect substrate preferences, since soft bottom areas in general would be less rough than hard bottom areas. The morphospecies positively correlated with temperature were in general negatively correlated with slope and roughness, and these were the species that had high densities in the Barite field, a soft bottom habitat. Aspect was not statistically significant in determining species distributions.

4.6 Comparison with other sites along the Arctic Mid-Ocean Ridge

Benthic community studies for the AMOR are still scarce, in particular for active vents, therefore formal comparisons are not straightforward. The most comprehensive reference study using video analysis is that of Ramirez-Llodra *et al.* (2020) on the inactive sulphide mound Mohn's treasure, situated 30 km away from Loki's Castle. Few morphospecies were recorded at Loki's Castle compared to the 46 morphospecies recorded at Mohn' Treasure. However, as earlier noted, there are several species known to inhabit Loki's Castle and other vents on the AMOR that could not be recorded in this study due to image resolution limitations.

Some typical background taxa that were recorded at Loki's Castle are also found at other AMOR sites. Anemones are prominent megafauna in the communities at shallow hydrothermal

vents at Mohn's ridge (Schander *et al.*, 2010). *Bythocaris* shrimp are recorded from Mohn's Treasure (Ramirez-Llodra *et al.*, 2020) and are ubiquitous in underwater surveys throughout the AMOR. Buccinid gastropods are present in the background community at Håkon Mosby mud volcano and Mohn's treasure (Gebruk *et al.*, 2003; Ramirez-Llodra *et al.*, 2020), as well as other soft sediment areas on the AMOR (P. Ribeiro, personal communication). The vent-endemic *S. contortum* has a wide distribution from the Arctic to the Antarctic (Eilertsen *et al.*, 2018), and in the Arctic it is known from Håkon Mosby mud volcano (Smirnov, 2000; Gebruk *et al.*, 2003). The presence of shared taxa indicates that there could be some connectivity between these sites. No particular morphospecies appears to be restricted to Loki's Castle, but the community on the Barite field is unique.

Dense aggregations of sponges are also observed on the Schultz Bank, Mohn's Treasure and hydrothermal vents at Mohn's ridge (Schander *et al.*, 2010; Meyer *et al.*, 2019; Ramirez-Llodra *et al.*, 2020). Except for a few individuals of *A. megaatrialia*, carnivorous sponges of the family Cladorhizidae and a third unidentified sponge, the sponge community observed at Loki's Castle is dominated by one small-sized morphospecies, which is also very common in other basaltic areas of the ridge (P. Ribeiro, personal communication). The sponge community around hydrothermal vents at Mohn's ridge is also characterized by very small sponges, mainly Cladorhizidae and Calcarea (Schander *et al.*, 2010), while the most abundant sponges at Loki's Castle and other deeper hydrothermal vents such as Fåvne most likely belong to the class Demospongiae (P. Ribeiro, personal communication). The Schulz Bank displays a more diverse sponge community (Meyer *et al.*, 2019). A significant difference between the faunal community at Loki's Castle and the communities at Mohn's Treasure and Håkon Mosby mud volcano is that these two sites have a high abundance of echinoderms (Gebruk *et al.*, 2003; Ramirez-Llodra *et al.*, 2020). In contrast, only a few individuals of Crinoidea and Asteroidea were recorded at Loki's Castle, but the surveyed area was much smaller at Loki's Castle than at the other sites.

4.7 Implications for environmental management of seabed mining

This thesis provides an overview of the diversity, abundance, density and spatial distribution of the benthic macrofauna at Loki's Castle. This is baseline information that can be useful when assessing how a possible future SMS mining event at or near Loki's Castle will impact

the faunal community. As previous studies also have shown, the fauna at Loki's Castle is specialized and highly endemic on a regional scale (Pedersen *et al.*, 2010; Tandberg *et al.*, 2012; Kongsrud *et al.*, 2017), and SMS mining in this vent field would be critical to the fauna inhabiting Loki's Castle. SMS mining at active sites would directly eliminate vital habitat for a number of species and could alter the hydrothermal circulation from vents (Ramirez-Llodra *et al.*, 2011; Van Dover, 2011; Jamieson & Gartman, 2020). Since hydrothermal fluids and temperature are important structuring factors of faunal distribution, this could completely change the benthic community at the site. More knowledge about connectivity is also needed to predict the different species ability to recolonize after a disturbance.

The sponge community found in the periphery of Loki's Castle could also be affected by a mining event. Deep sea sponge aggregations are on the list of vulnerable marine ecosystems (FAO, 2019). They are sensitive to increased turbidity, and take long time to recover due to their slow growth rate (Comission, 2010). Some deep-sea sponge species actively remove bioavailable nutrients from the ecosystem, and disturbance from an event such as SMS mining could completely alter this ecosystem function (Rooks *et al.*, 2020).

5. Concluding remarks

The composition of benthic macrofauna at Loki's Castle clearly differs between focused venting areas, diffuse venting areas and the periphery. The five study sites had different morphospecies assemblages, densities and diversity. The spatial distribution of most morphospecies is influenced by temperature, or likely co-varying parameters, while slope seems to be less important. Temperature and slope can also explain some of the difference in total density and species richness between sites. However, much of the difference is likely also influenced by other abiotic and biological factors, such as vent fluid toxicity, substrate, food availability, competition and predation. The influence of these factors in shaping benthic communities at Loki's Castle should be the focus of future studies.

The community at the Barite field was clearly different from the other sites, due to the presence of vent-endemic fauna. This site also had the highest density and diversity of all sites. The intermediate-stress conditions and the facilitation by *S.contortum* might promote density and diversity in the Barite field. It is possible that the proximity to the Barite field contributes to the higher density and diversity seen at the Eastern sites compared to the Western sites. Vent fluid direction and substrate might also account for this difference.

The benthic megafauna community at Loki's Castle displays less morphospecies compared to other sites studied at the AMOR, but the community at the Barite field is unique and hosts several vent-endemic species. Possible future SMS mining events at or near Loki's Castle will likely impact this specialized fauna. This thesis provides baseline knowledge of the benthic fauna and its spatial distribution patterns that can be used in assessing the faunal community's susceptibility to a mining event. In addition, similar studies should be conducted on other sites along the AMOR for a more complete picture of the degree of biogeographical connectivity of these communities. From a conservation perspective, this information would be crucial to understand how hydrothermal vent and peripheral habitats can be impacted by seabed mining and other human activities, and to find ways to mitigate those impacts.

Bibliography

Adams, D.K., Arellano, S.M. & Govenar, B. (2012) Larval dispersal: vent life in the water column. *Oceanography* **25**, 256–268.

Aguzzi, J., Jamieson, A., Fujii, T., Sbragaglia, V., Costa, C., Menesatti, P. & Fujiwara, Y. (2012) Shifting feeding behaviour of deep-sea buccinid gastropods at natural and simulated food falls. *Marine Ecology Progress Series* **458**, 247–253.

Arquit, A.M. (1990) Geological and hydrothermal controls on the distribution of megafauna in Ashes Vent Field, Juan de Fuca Ridge. *Journal of Geophysical Research: Solid Earth* **95**, 12947–12960.

Baco, A.R., Etter, R.J., Ribeiro, P.A., Von der Heyden, S., Beerli, P. & Kinlan, B.P. (2016) A synthesis of genetic connectivity in deep-sea fauna and implications for marine reserve design. *Molecular Ecology* **25**, 3276–3298.

Baco, A.R. & Smith, C.R. (2003) High species richness in deep-sea chemoautotrophic whale skeleton communities. *Marine Ecology Progress Series* **260**, 109–114.

Barreyre, T., Escartín, J., Garcia, R., Cannat, M., Mittelstaedt, E. & Prados, R. (2012) Structure, temporal evolution, and heat flux estimates from the Lucky Strike deep-sea hydrothermal field derived from seafloor image mosaics. *Geochemistry, Geophysics, Geosystems* **13**.

Bates, A.E., Lee, R.W., Tunnicliffe, V. & Lamare, M.D. (2010) Deep-sea hydrothermal vent animals seek cool fluids in a highly variable thermal environment. *Nature Communications* **1**, 1–6.

Bates, A.E., Tunnicliffe, V. & Lee, R.W. (2005) Role of thermal conditions in habitat selection by hydrothermal vent gastropods. *Marine Ecology Progress Series* **305**, 1–15.

Baumberger, T., Früh-Green, G.L., Thorseth, I.H., Lilley, M.D., Hamelin, C., Bernasconi, S.M., Okland, I.E. & Pedersen, R.B. (2016) Fluid composition of the sediment-influenced Loki's Castle vent field at the ultra-slow spreading Arctic Mid-Ocean Ridge. *Geochimica et Cosmochimica Acta* **187**, 156–178.

Bell, J.B., Woulds, C., Brown, L.E., Sweeting, C.J., Reid, W.D., Little, C.T. & Glover, A.G. (2016) Macrofaunal ecology of sedimented hydrothermal vents in the Bransfield Strait, Antarctica. *Frontiers in Marine Science* **3**, 32.

Bernardino, A.F., Levin, L.A., Thurber, A.R. & Smith, C.R. (2012) Comparative composition, diversity and trophic ecology of sediment macrofauna at vents, seeps and organic falls. *PLoS One* **7**, e33515.

Bienhold, C., Ristova, P.P., Wenzhöfer, F., Dittmar, T. & Boetius, A. (2013) How deep-sea wood falls sustain chemosynthetic life. *PloS one* **8**, e53590.

Boschen, R.E., Rowden, A.A., Clark, M.R. & Gardner, J.P. (2013) Mining of deep-sea seafloor massive sulfides: a review of the deposits, their benthic communities, impacts from mining, regulatory frameworks and management strategies. *Ocean & coastal management* **84**, 54–67.

Breusing, C., Biastoch, A., Drews, A., Metaxas, A., Jollivet, D., Vrijenhoek, R.C., Bayer, T., Melzner, F., Sayavedra, L., Petersen, J.M. *et al.* (2016) Biophysical and population genetic models predict the presence of "phantom" stepping stones connecting Mid-Atlantic Ridge vent ecosystems. *Current Biology* **26**, 2257–2267.

Caldeira, K. & Wickett, M.E. (2003) Anthropogenic carbon and ocean pH. *Nature* **425**, 365–365.

Cathles, L.M. (2011) What processes at mid-ocean ridges tell us about volcanogenic massive sulfide deposits. *Mineralium Deposita* **46**, 639–657.

Chapman, A.S., Beaulieu, S.E., Colaço, A., Gebruk, A.V., Hilario, A., Kihara, T.C., Ramirez-Llodra, E., Sarrazin, J., Tunnicliffe, V., Amon, D.J. *et al.* (2019) sFDvent: A global trait database for deep-sea hydrothermal-vent fauna. *Global Ecology and Biogeography* **28**, 1538–1551.

Comission, O. (2010) Background document for deep sea sponge aggregations. Report.

Cuvelier, D., Sarrazin, J., Colaço, A., Copley, J., Desbruyères, D., Glover, A.G., Tyler, P. & Santos, R.S. (2009) Distribution and spatial variation of hydrothermal faunal assemblages at Lucky Strike (Mid-Atlantic Ridge) revealed by high-resolution video image analysis. *Deep Sea Research Part I: Oceanographic Research Papers* **56**, 2026–2040.

Danovaro, R., Aguzzi, J., Fanelli, E., Billett, D., Gjerde, K., Jamieson, A., Ramirez-Llodra, E., Smith, C., Snelgrove, P., Thomsen, L. *et al.* (2017) An ecosystem-based deep-ocean strategy. *Science* **355**, 452–454.

Danovaro, R., Fanelli, E., Aguzzi, J., Billett, D., Carugati, L., Corinaldesi, C., Dell'Anno, A., Gjerde, K., Jamieson, A.J., Kark, S. *et al.* (2020) Ecological variables for developing a global deep-ocean monitoring and conservation strategy. *Nature ecology & evolution* **4**, 181–192.

Decker, C., Morineaux, M., Van Gaever, S., Caprais, J., Lichtschlag, A., Gauthier, O., Andersen, A.C. & Olu, K. (2012) Habitat heterogeneity influences cold-seep macrofaunal communities within and among seeps along the Norwegian margin. Part 1: Macrofaunal community structure. *Marine Ecology* **33**, 205–230.

Desbruyères, D., Hashimoto, J. & Fabri, M.C. (2006) *Composition and Biogeography of Hydrothermal Vent Communities in Western Pacific Back-Arc Basins*, pp. 215–234. American Geophysical Union (AGU).

Dick, H.J., Lin, J. & Schouten, H. (2003) An ultraslow-spreading class of ocean ridge. *Nature* **426**, 405–412.

Dinno, A. (2017) *Package 'dunn. test'*.

Dunn, D.C., Van Dover, C.L., Etter, R.J., Smith, C.R., Levin, L.A., Morato, T., Colaço, A., Dale, A.C., Gebruk, A.V., Gjerde, K.M. *et al.* (2018) A strategy for the conservation of biodiversity on mid-ocean ridges from deep-sea mining. *Science advances* **4**, eaar4313.

Eilertsen, M.H., Georgieva, M.N., Kongsrud, J.A., Linse, K., Wiklund, H., Glover, A.G. & Rapp, H.T. (2018) Genetic connectivity from the Arctic to the Antarctic: *Sclerolinum contortum* and *Nicomache lokii* (Annelida) are both widespread in reducing environments. *Scientific reports* **8**, 1–12.

Eilertsen, M.H., Kongsrud, J.A., Alvestad, T., Stiller, J., Rouse, G.W. & Rapp, H.T. (2017) Do ampharetids take sedimented steps between vents and seeps? Phylogeny and habitat-use

of Ampharetidae (Annelida, Terebelliformia) in chemosynthesis-based ecosystems. *BMC evolutionary biology* **17**, 1–15.

Erickson, K., Macko, S. & Van Dover, C. (2009) Evidence for a chemoautotrophically based food web at inactive hydrothermal vents (Manus Basin). *Deep Sea Research Part II: Topical Studies in Oceanography* **56**, 1577–1585.

Escartín, J., Garcia, R., Delaunoy, O., Ferrer, J., Gracias, N., Elibol, A., Cufi, X., Neumann, L., Fornari, D., Humphris, S. *et al.* (2008) Globally aligned photomosaic of the Lucky Strike hydrothermal vent field (Mid-Atlantic Ridge, 37 18.5' N): Release of georeferenced data, mosaic construction, and viewing software. *Geochemistry, Geophysics, Geosystems* **9**.

FAO (2019) VME indicators, thresholds and encounter responses adopted by R(F)Mos in force during 2019.

Fisher, C.R., Takai, K. & Le Bris, N. (2007) Hydrothermal vent ecosystems. *Oceanography* **20**, 14–23.

Galkin, S. (1997) Megafauna associated with hydrothermal vents in the Manus back-arc Basin (Bismarck Sea). *Marine Geology* **142**, 197–206.

Gebruk, A.V., Krylova, E.M., Lein, A.Y., Vinogradov, G.M., Anderson, E., Pimenov, N.V., Cherkashev, G.A. & Crane, K. (2003) Methane seep community of the Håkon Mosby mud volcano (the Norwegian Sea): composition and trophic aspects. *Sarsia* **88**, 394–403.

Georgieva, M.N., Taboada, S., Riesgo, A., Díez-Vives, C., De Leo, F.C., Jeffreys, R.M., Copley, J.T., Little, C.T., Ríos, P. & Cristobo, J. (2020) Evidence of vent-adaptation in sponges living at the periphery of hydrothermal vent environments: ecological and evolutionary implications. *Frontiers in microbiology* **11**, 1636.

Georgieva, M.N., Wiklund, H., Bell, J.B., Eilertsen, M.H., Mills, R.A., Little, C.T. & Glover, A.G. (2015) A chemosynthetic weed: the tubeworm *Sclerolinum contortum* is a bipolar, cosmopolitan species. *BMC Evolutionary Biology* **15**, 1–17.

Gerdes, K., Martínez Arbizu, P., Schwarz-Schampera, U., Schwentner, M. & Kihara, T.C. (2019) Detailed mapping of hydrothermal vent fauna: a 3D reconstruction approach based on video imagery. *Frontiers in Marine Science* **6**, 96.

Girona Underwater Vision and Robotics (2014) MosaicViewer.

Goffredi, S.K., Johnson, S., Tunnicliffe, V., Caress, D., Clague, D., Escobar, E., Lundsten, L., Paduan, J.B., Rouse, G. & Salcedo, D.L. (2017) Hydrothermal vent fields discovered in the southern Gulf of California clarify role of habitat in augmenting regional diversity. *Proceedings of the Royal Society B: Biological Sciences* **284**, 20170817.

Goffredi, S.K., Motooka, C., Fike, D.A., Gusmão, L.C., Tilic, E., Rouse, G.W. & Rodríguez, E. (2021) Mixotrophic chemosynthesis in a deep-sea anemone from hydrothermal vents in the Pescadero Basin, Gulf of California. *BMC biology* **19**, 1–18.

Gollner, S., Govenar, B., Fisher, C.R. & Bright, M. (2015) Size matters at deep-sea hydrothermal vents: different diversity and habitat fidelity patterns of meio-and macrofauna. *Marine ecology progress series* **520**, 57–66.

Gollner, S., Kaiser, S., Menzel, L., Jones, D.O., Brown, A., Mestre, N.C., Van Oevelen, D., Menot, L., Colaço, A. & Canals, M. (2017) Resilience of benthic deep-sea fauna to mining activities. *Marine Environmental Research* **129**, 76–101.

Hannington, M. & Monecke, T. (2009) Global exploration models for polymetallic sulphides in the Area: An assessment of lease block selection under the draft regulations on prospecting and exploration for polymetallic sulphides. *Marine Georesources and Geotechnology* **27**, 132–159.

Harrell Jr, F.E. (2019) Package 'hmisc'.

Horton, T., Marsh, L., Bett, B.J., Gates, A.R., Jones, D.O.B., Benoist, N.M.A., Pfeifer, S., Simon-Lledó, E., Durden, J.M., Vandepitte, L. & Appeltans, W. (2021) Recommendations for the standardisation of open taxonomic nomenclature for image-based identifications. *Frontiers in Marine Science* **8**.

International Seabed Authority (2021) Exploration contracts.

Jaeschke, A., Jørgensen, S., Bernasconi, S.M., Pedersen, R.B., Thorseth, I.H. & Früh-Green, G.L. (2012) Microbial diversity of Loki's Castle black smokers at the Arctic Mid-Ocean Ridge. *Geobiology* **10**, 548–561.

Jamieson, J.W. & Gartman, A. (2020) Defining active, inactive, and extinct seafloor massive sulfide deposits. *Marine Policy* **117**, 103926.

Johnson, K.S., Childress, J.J. & Beehler, C.L. (1988) Short-term temperature variability in the Rose Garden hydrothermal vent field: an unstable deep-sea environment. *Deep Sea Research Part A. Oceanographic Research Papers* **35**, 1711–1721.

Jones, K. & Wrigley, N. (1995) Generalized additive models, graphical diagnostics, and logistic regression. *Geographical Analysis* **27**, 1–18.

Keeling, R.F., Körtzinger, A. & Gruber, N. (2010) Ocean deoxygenation in a warming world. *Annual review of marine science* **2**, 199–229.

Kim, S. & Hammerstrom, K. (2012) Hydrothermal vent community zonation along environmental gradients at the Lau back-arc spreading center. *Deep Sea Research Part I: Oceanographic Research Papers* **62**, 10–19.

Klunder, L., De Stigter, H., Lavaleye, M.S., Van Bleijswijk, J.D., Van Der Veer, H.W., Reichart, G.J. & Duineveld, G.C. (2020) A molecular approach to explore the background benthic fauna around a hydrothermal vent and their larvae: Implications for future mining of deep-sea SMS deposits. *Frontiers in Marine Science* .

Kongsrud, J.A., Eilertsen, M.H., Alvestad, T., Kongshavn, K. & Rapp, H.T. (2017) New species of Ampharetidae (Annelida: Polychaeta) from the Arctic Loki Castle vent field. *Deep Sea Research Part II: Topical Studies in Oceanography* **137**, 232–245.

Kongsrud, J.A. & Rapp, H.T. (2012) *Nicomache (Loxochona) lokii* sp. nov.(Annelida: Polychaeta: Maldanidae) from the Loki's Castle vent field: an important structure builder in an Arctic vent system. *Polar biology* **35**, 161–170.

Lee, R.W. (2003) Thermal tolerances of deep-sea hydrothermal vent animals from the Northeast Pacific. *The Biological Bulletin* **205**, 98–101.

Levesque, C., Juniper, S.K. & Marcus, J. (2003) Food resource partitioning and competition among alvinellid polychaetes of Juan de Fuca Ridge hydrothermal vents. *Marine Ecology Progress Series* **246**, 173–182.

Levin, L.A. (2019) Sustainability in deep water. *Oceanography* **32**, 170–180.

Levin, L.A. & Le Bris, N. (2015) The deep ocean under climate change. *Science* **350**, 766–768.

Lösekann, T., Robador, A., Niemann, H., Knittel, K., Boetius, A. & Dubilier, N. (2008) Endosymbioses between bacteria and deep-sea siboglinid tubeworms from an Arctic cold seep (Haakon Mosby Mud Volcano, Barents Sea). *Environmental Microbiology* **10**, 3237–3254.

Luther, G.W., Rozan, T.F., Taillefert, M., Nuzzio, D.B., Di Meo, C., Shank, T.M., Lutz, R.A. & Cary, S.C. (2001) Chemical speciation drives hydrothermal vent ecology. *Nature* **410**, 813–816.

Marsh, A.G., Mullineaux, L.S., Young, C.M. & Manahan, D.T. (2001) Larval dispersal potential of the tubeworm *Riftia pachyptila* at deep-sea hydrothermal vents. *Nature* **411**, 77–80.

Martinez Arbizu, P. (2020) pairwiseAdonis: Pairwise multilevel comparison using adonis.

McClain, C.R. & Schlacher, T.A. (2015) On some hypotheses of diversity of animal life at great depths on the sea floor. *Marine Ecology* **36**, 849–872.

McMullin, E.R., Bergquist, D.C. & Fisher, C.R. (2007) Metazoans in extreme environments: adaptations of hydrothermal vent and hydrocarbon seep fauna. *Gravitational and Space Research* **13**.

Mecklenburg, C., Lynghammar, A., Johannesen, E., Byrkjedal, I., Christiansen, J., Dolgov, A., Karamushko, O., Mecklenburg, T., Møller, P., Steinke, D. & Wienerroither, R. (2018) Marine fishes of the Arctic region. Report, Conservation of Arctic Flora and Fauna.

Meyer, H.K., Roberts, E.M., Rapp, H.T. & Davies, A.J. (2019) Spatial patterns of arctic sponge ground fauna and demersal fish are detectable in autonomous underwater vehicle (AUV) imagery. *Deep Sea Research Part I: Oceanographic Research Papers* **153**, 103137.

Micheli, F., Peterson, C.H., Mullineaux, L.S., Fisher, C.R., Mills, S.W., Sancho, G., Johnson, G.A. & Lenihan, H.S. (2002) Predation structures communities at deep-sea hydrothermal vents. *Ecological monographs* **72**, 365–382.

Moalic, Y., Desbruyères, D., Duarte, C.M., Rozenfeld, A.F., Bachraty, C. & Arnaud-Haond, S. (2012) Biogeography revisited with network theory: retracing the history of hydrothermal vent communities. *Systematic Biology* **61**, 127.

Mullineaux, L.S., Adams, D.K., Mills, S.W. & Beaulieu, S.E. (2010) Larvae from afar colonize deep-sea hydrothermal vents after a catastrophic eruption. *Proceedings of the National Academy of Sciences* **107**, 7829–7834.

Mullineaux, L.S., Metaxas, A., Beaulieu, S.E., Bright, M., Gollner, S., Grupe, B.M., Herrera, S., Kellner, J.B., Levin, L.A. & Mitarai, S. (2018) Exploring the ecology of deep-sea hydrothermal vents in a metacommunity framework. *Frontiers in Marine Science* **5**, 49.

Nakamura, K. & Takai, K. (2014) Theoretical constraints of physical and chemical properties of hydrothermal fluids on variations in chemolithotrophic microbial communities in seafloor hydrothermal systems. *Progress in Earth and Planetary Science* **1**, 5.

Oksanen, J., Blanchet, F.G., Kindt, R., Legendre, P., Minchin, P.R., O'hara, R., Simpson, G.L., Solymos, P., Stevens, M.H.H., Wagner, H. *et al.* (2013) Package 'vegan'. *Community ecology package, version* **2**, 1–295.

Olsen, B.R., Troedsson, C., Hadziavdic, K., Pedersen, R.B. & Rapp, H.T. (2014) A molecular gut content study of *Themisto abyssorum* (Amphipoda) from Arctic hydrothermal vent and cold seep systems. *Molecular ecology* **23**, 3877–3889.

Olsen, B.R., Troedsson, C., Hadziavdic, K., Pedersen, R.B. & Rapp, H.T. (2015) The influence of vent systems on pelagic eukaryotic micro-organism composition in the Nordic Seas. *Polar Biology* **38**, 547–558.

Pedersen, R.B. & Bjerkgård, T. (2016) Seafloor massive sulphides in Arctic waters. *Mineral Resources In The Arctic* **1**, 209–216.

Pedersen, R.B., Rapp, H.T., Thorseth, I.H., Lilley, M.D., Barriga, F.J., Baumberger, T., Flesland, K., Fonseca, R., Früh-Green, G.L. & Jorgensen, S.L. (2010) Discovery of a black smoker vent field and vent fauna at the Arctic Mid-Ocean Ridge. *Nature Communications* **1**, 1–6.

Petersen, S., Krätschell, A., Augustin, N., Jamieson, J., Hein, J.R. & Hannington, M.D. (2016) News from the seabed - Geological characteristics and resource potential of deep-sea mineral resources. *Marine Policy* **70**, 175–187.

Podowski, E.L., Ma, S., Luther III, G.W., Wardrop, D. & Fisher, C.R. (2010) Biotic and abiotic factors affecting distributions of megafauna in diffuse flow on andesite and basalt along the eastern lau spreading center, tonga. *Marine Ecology Progress Series* **418**, 25–45.

Portail, M., Olu, K., Escobar-Briones, E., Caprais, J.C., Menot, L., Waeles, M., Cruaud, P., Sarradin, P.M., Godfroy, A. & Sarrazin, J. (2015) Comparative study of vent and seep macrofaunal communities in the Guaymas Basin. *Biogeosciences* **12**, 5455–5479.

QGIS Development Team (2009) QGIS Geographic Information System.

R Development Core Team (2010) R: A language and environment for statistical computing.

Ramirez-Llodra, E., Brandt, A., Danovaro, R., Mol, B.D., Escobar, E., German, C.R., Levin, L.A., Martinez Arbizu, P., Menot, L. & Buhl-Mortensen, P. (2010) Deep, diverse and definitely different: unique attributes of the world's largest ecosystem. *Biogeosciences* **7**, 2851–2899.

Ramirez-Llodra, E., Hilario, A., Paulsen, E., Costa, C., Johnsen, G., Bakken, T. & Rapp, H.T. (2020) Benthic communities on the Mohn's Treasure mound: implications for management of seabed mining in the Arctic Mid-Ocean Ridge. *Frontiers in Marine Science* **7**, 490.

Ramirez-Llodra, E., Shank, T.M. & German, C.R. (2007) Biodiversity and biogeography of hydrothermal vent species: thirty years of discovery and investigations. *Oceanography* **20**, 30–41.

Ramirez-Llodra, E., Tyler, P.A., Baker, M.C., Bergstad, O.A., Clark, M.R., Escobar, E., Levin, L.A., Menot, L., Rowden, A.A. & Smith, C.R. (2011) Man and the last great wilderness: human impact on the deep sea. *PLoS one* **6**, e22588.

Ramsay, T.O., Burnett, R.T. & Krewski, D. (2003) The effect of concurvity in generalized additive models linking mortality to ambient particulate matter. *Epidemiology* **14**, 18–23.

Rikter-Svendsen, R. (2020) Distribution of thermochemical output and associated ecosystems at the Loki's Castle hydrothermal field.

Rooks, C., Fang, J.K.H., Mørkved, P.T., Zhao, R., Rapp, H.T., Xavier, J.R. & Hoffmann, F. (2020) Deep-sea sponge grounds as nutrient sinks: denitrification is common in boreo-Arctic sponges. *Biogeosciences* **17**, 1231–1245.

RStudio Team (2016) *RStudio: Integrated Development Environment for R*. RStudio, Inc., Boston, MA.

Sancho, G., Fisher, C., Mills, S., Micheli, F., Johnson, G., Lenihan, H., Peterson, C. & Mullineaux, L. (2005) Selective predation by the zoarcid fish *Thermarces cerberus* at hydrothermal vents. *Deep Sea Research Part I: Oceanographic Research Papers* **52**, 837–844.

Sarrazin, J., Juniper, S.K., Massoth, G. & Legendre, P. (1999) Physical and chemical factors influencing species distributions on hydrothermal sulfide edifices of the Juan de Fuca Ridge, northeast Pacific. *Marine Ecology Progress Series* **190**, 89–112.

Schander, C., Rapp, H.T., Kongsrud, J.A., Bakken, T., Berge, J., Cochrane, S., Oug, E., Byrkjedal, I., Todt, C. & Cedhagen, T. (2010) The fauna of hydrothermal vents on the Mohn Ridge (North Atlantic). *Marine Biology Research* **6**, 155–171.

Schulte, M. (2007) The emergence of life on earth. *Oceanography* **20**, 42–49.

Seabed Mineral Law (2019) Law on mineral activities on the continental shelf.

Sen, A., Kim, S., Miller, A.J., Hovey, K.J., Hourdez, S., Luther III, G.W. & Fisher, C.R. (2016) Peripheral communities of the Eastern Lau Spreading Center and Valu Fa Ridge: community composition, temporal change and comparison to near-vent communities. *Marine Ecology* **37**, 599–617.

Sibuet, M. & Olu, K. (1998) Biogeography, biodiversity and fluid dependence of deep-sea cold-seep communities at active and passive margins. *Deep Sea Research Part II: Topical Studies in Oceanography* **45**, 517–567.

Sievert, S.M. & Vetriani, C. (2012) Chemoautotrophy at deep-sea vents: past, present, and future. *Oceanography* **25**, 218–233.

Smirnov, R.V. (2000) Two new species of Pogonophora from the arctic mud volcano off northwestern Norway. *Sarsia* **85**, 141–150.

Steen, I.H., Dahle, H., Stokke, R., Roalkvam, I., Daae, F.L., Rapp, H.T., Pedersen, R.B. & Thorseth, I.H. (2016) Novel barite chimneys at the Loki's Castle vent field shed light on key factors shaping microbial communities and functions in hydrothermal systems. *Frontiers in microbiology* **6**, 1510.

Stokke, R., Reeves, E.P., Dahle, H., Fedøy, A.E., Viflot, T., Lie Onstad, S., Vulcano, F., Pedersen, R.B., Eijsink, V.G. & Steen, I.H. (2020) Tailoring hydrothermal vent biodiversity toward improved biodiscovery using a novel in situ enrichment strategy. *Frontiers in Microbiology* **11**, 249.

Stuart, C.T. & Rex, M.A. (2009) Bathymetric patterns of deep-sea gastropod species diversity in 10 basins of the Atlantic Ocean and Norwegian Sea. *Marine Ecology* **30**, 164–180.

Svavarsson, J., Stromberg, J.O. & Brattegard, T. (1993) The deep-sea asellote (Isopoda, Crustacea) fauna of the Northern Seas: species composition, distributional patterns and origin. *Journal of Biogeography* pp. 537–555.

Sweetman, A.K., Levin, L.A., Rapp, H.T. & Schander, C. (2013) Faunal trophic structure at hydrothermal vents on the southern Mohn's Ridge, Arctic Ocean. *Marine Ecology Progress Series* **473**, 115–131.

Tandberg, A., Vader, W., Olsen, B. & Rapp, H. (2018) *Monoculodes bousfieldi* sp. n. from the Arctic hydrothermal vent Loki's Castle. *Marine Biodiversity* **48**, 927–937.

Tandberg, A.H., Rapp, H.T., Schander, C., Vader, W., Sweetman, A.K. & Berge, J. (2012) *Exitomelita sigynae* gen. et sp. nov.: a new amphipod from the Arctic Loki Castle vent field with potential gill ectosymbionts. *Polar biology* **35**, 705–716.

Treude, T., Smith, C.R., Wenzhöfer, F., Carney, E., Bernardino, A.F., Hannides, A.K., Krüger, M. & Boetius, A. (2009) Biogeochemistry of a deep-sea whale fall: sulfate reduction, sulfide efflux and methanogenesis. *Marine Ecology Progress Series* **382**, 1–21.

Tunnicliffe, V., Juniper, S.K. & Sibuet, M. (2003) Reducing environments of the deep-sea floor. *Ecosystems of the World* pp. 81–110.

Tyler, P.A. (2003) *Ecosystems of the deep oceans*. Elsevier.

Tyler, P.A. & Young, C.M. (2003) Dispersal at hydrothermal vents: a summary of recent progress. *Hydrobiologia* **503**, 9–19.

Van Dover, C., Colaço, A., Collins, P., Croot, P., Metaxas, A., Murton, B., Swaddling, A., Boschen-Rose, R., Carlsson, J. & Cuyvers, L. (2020) Research is needed to inform environmental management of hydrothermally inactive and extinct polymetallic sulfide (PMS) deposits. *Marine Policy* **121**, 104183.

Van Dover, C.L. (2011) Mining seafloor massive sulphides and biodiversity: what is at risk? *ICES Journal of Marine Science* **68**, 341–348.

Van Dover, C.L. (2019) Inactive sulfide ecosystems in the deep sea: a review. *Frontiers in Marine Science* **6**, 461.

Van Dover, C.L., Arnaud-Haond, S., Gianni, M., Helmreich, S., Huber, J.A., Jaeckel, A., Metaxas, A., Pendleton, L.H., Petersen, S. & Ramirez-Llodra, E. (2018) Scientific rationale

and international obligations for protection of active hydrothermal vent ecosystems from deep-sea mining. *Marine Policy* **90**, 20–28.

Van Dover, C.L., German, C., Speer, K.G., Parson, L. & Vrijenhoek, R. (2002) Evolution and biogeography of deep-sea vent and seep invertebrates. *science* **295**, 1253–1257.

Vrijenhoek, R.C. (2010) Genetic diversity and connectivity of deep-sea hydrothermal vent metapopulations. *Molecular ecology* **19**, 4391–4411.

Watanabe, H., Kado, R., Tsuchida, S., Miyake, H., Kyo, M. & Kojima, S. (2004) Larval development and intermoult period of the hydrothermal vent barnacle Neoverruca sp. *Marine Biological Association of the United Kingdom. Journal of the Marine Biological Association of the United Kingdom* **84**, 743.

Wickham, H. (2016) *ggplot2: Elegant Graphics for Data Analysis*. Springer-Verlag New York.

Wickham, H., Francois, R., Henry, L. & Müller, K. (2015) dplyr: A grammar of data manipulation. *R package version 0.4* **3**, p156.

Wienerroither, R.M., Nedreaas, K.H., Uiblein, F., Christiansen, J.S., Byrkjedal, I. & Karamushko, O. (2011) The marine fishes of Jan Mayen Island, NE Atlantic - past and present. *Marine Biodiversity* **41**, 395–411.

Appendices

A. Temperature and heat flux

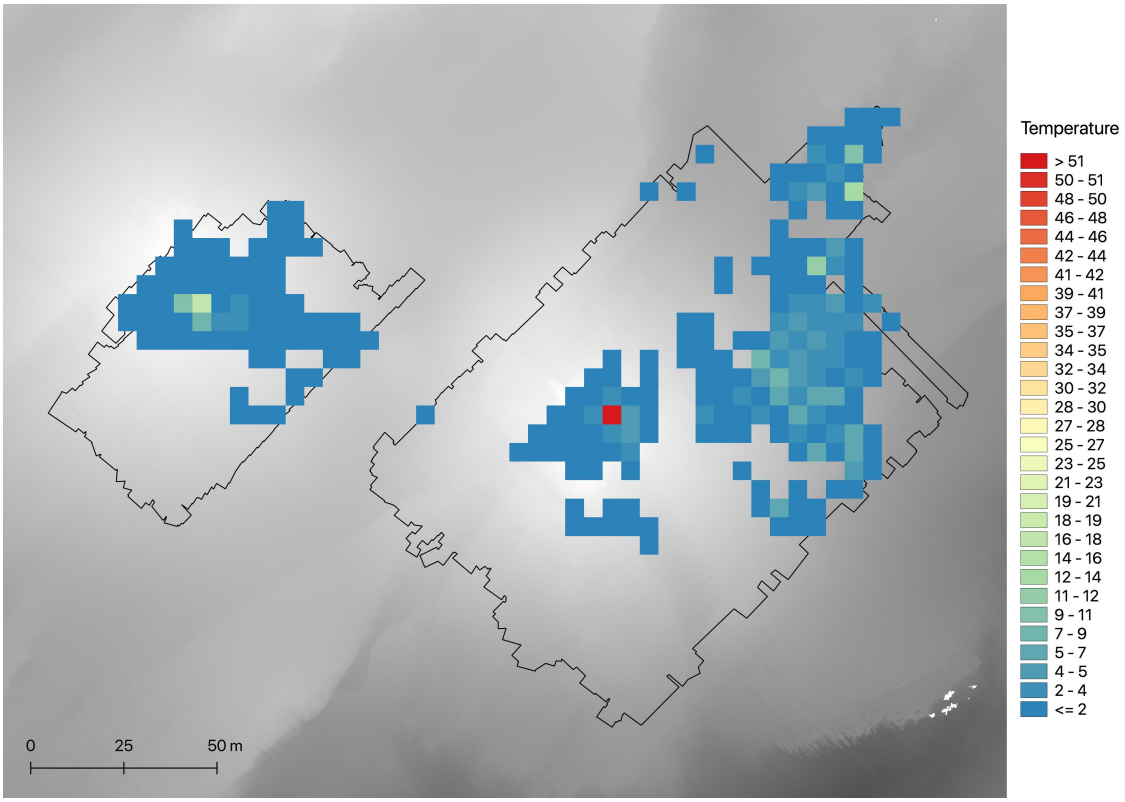

Figure A.1: Average temperature above the ambient sea water. Each square represents 5x5m, lines represent photomosaic boundaries.

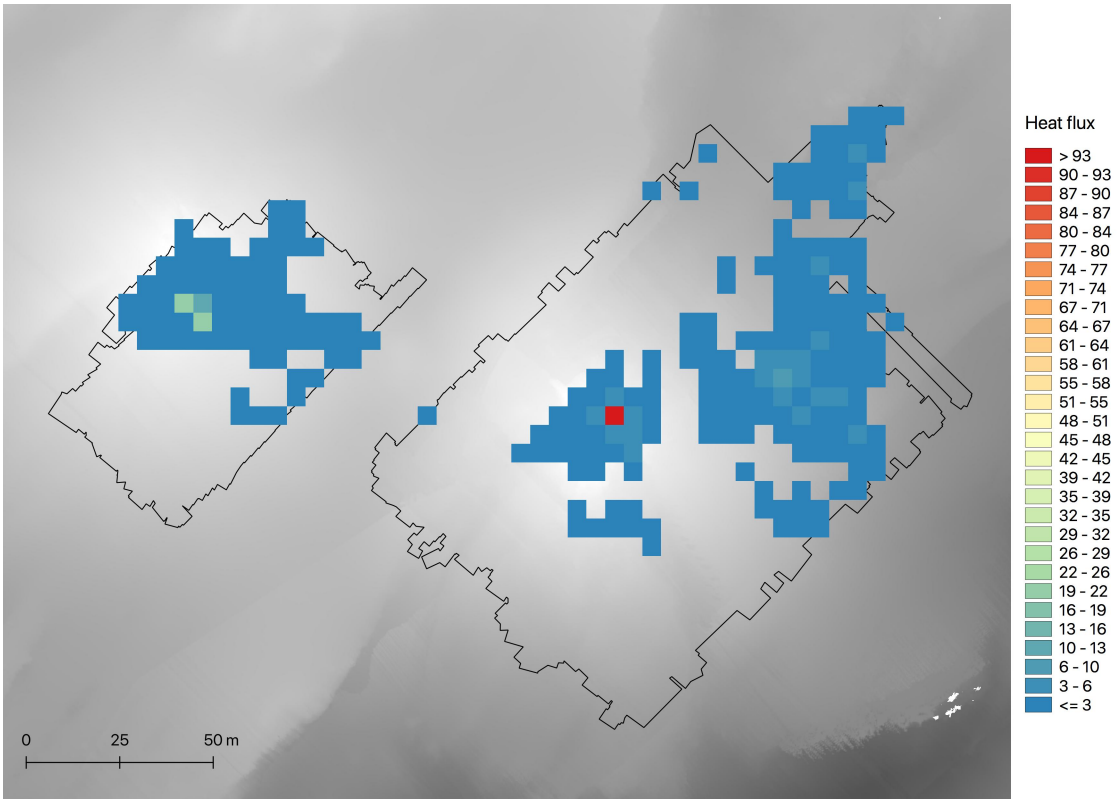

Figure A.2: Average heat flux. Each square represents 5x5m, lines represent photomosaic boundaries.

B. R script

```
1
2  # Packages
3  library(vegan)
4  library(ggplot2)
5  library(ggsci)
6  library(RColorBrewer)
7  library(Hmisc)
8  library(dplyr)
9  library(mgcv)
10 library(plotrix)
11 library(car)
12 library(rlang)
13 library(dunn.test)
14
15 # Import data
16 mastertable.df <- read.table("mastertable_final.csv", header=T, sep=";",
17                              dec=".")
18
19 density.df <- read.table("densities.csv", header=T, sep=";",
20                              dec=".")
21
22 percentage.df <- read.table("percentage.csv", header=T, sep=";",
23                             dec=".")
24
25 counts.df <- read.table("counts.csv", header=T, sep=";",
26                            dec=".")
27
28 # Abundance per site
29 abundance.site <- counts2.df %>%
30   group_by(site) %>%
31   summarise_at(vars(-id, -site1), funs(sum(., na.rm=TRUE)))
32
33 # Mean and SE density
34 mean.den <- density.df %>%
35   group_by(site) %>%
36   summarise_at(vars(-id), funs(mean(., na.rm=TRUE)))
37
38 stdev.den <- density.df %>%
39   group_by(site) %>%
40   summarise_at(vars(-id), funs(std.error(., na.rm=TRUE)))
41
42
43 # Proportion plot
44 p0 <- ggplot(data=percentage.df, aes(x=site, y=percent_sqrt, fill=morphotype)) +
45   geom_bar(stat="identity")
46 p0 <- p0 + scale_fill_d3(palette = "category20", alpha = 0.8, name = "Morphospecies",
47 labels = c("Actiniaria stet. 1", "Actiniaria stet. 3", "Actiniaria stet. 2",
48 "Amphipoda stet.", "Asconema megaatrialia", "Cladorhizidae stet.",
49 "Crinoidea stet.", "Lycenchelys platyrhina", "Munnopsidae stet.",
50 "Sclerolinum contortum", "Asteroidea stet.", "Bythocaris sp. indet.",
51  "Buccinidae indet.", "Porifera indet. 1"))
52
```

```r
p0 <-p0 + labs(x="", y="Percentage relative density")
p0 <- p0 + theme(legend.text=element_text(size=15))
p0 <- p0 + theme_classic()
p0 <- p0 + theme(axis.text.x = element_text(size=12),
axis.text.y = element_text(size=12),
axis.title = element_text(size = 13))
p0 <- p0 + scale_x_discrete(labels=c("barite" = "Barite field",
"east_mound" = "Eastern mound",
"east_periphery" = "Eastern periphery", "west_mound" = "Western mound",
"west_periphery" = "Western periphery"))
p0


# Density plot
p1 <- ggplot(data=density.df, aes(x=site, y=sqrt_total, fill=site)) +
  geom_boxplot()
p1 <- p1 + theme_classic()
p1 <- p1 + labs(x="", y="Total relative density")
p1 <- p1 + scale_x_discrete(labels= c("Barite field", "Eastern mound",
"Eastern periphery", "Western mound", "Western periphery"))
p1 <- p1 + theme(legend.position = "none")
p1 <- p1 + theme(axis.text.x = element_text(size=15),
axis.text.y = element_text(size=12),
axis.title = element_text(size = 14))
p1 <- p1 + scale_fill_npg()
p1


# Diversity indices
species <- c("act_brown", "act_small", "act_large", "amphipod", "carnivorous",
"crinoid", "isopod", "seastar", "shrimp", "snail", "sponge", "asconema",
"eelpout", "tw_area")
species.df <- mastertable.df[species]

# Calculate no. of species for each row
mastertable.df$sp.no <- specnumber(species.df, MARGIN = 1)

# Calculate Shannon diversity for each row
mastertable.df$H <- diversity(species.df, index = "shannon",
MARGIN = 1, base = exp(1))

# Simpson diversity
mastertable.df$simpson <- diversity(species.df, index = "simpson",
MARGIN = 1, base = exp(1))

# Calculate evenness for each row
attach(mastertable.df)
mastertable.df$evenness <- H/log(sp.no)

# Mean and standard error diversity indices

# Shannon diversity index
mean.H <- mastertable.df %>%
  group_by(site) %>%
  summarise_at(vars(H), funs(mean(., na.rm=TRUE)))

std.error.H <- mastertable.df %>%
  group_by(site) %>%
  summarise_at(vars(H), funs(std.error(., na.rm=TRUE)))

# Simpson diversity index

mean.simpson <- mastertable.df %>%
```

```
  group_by(site) %>%
  summarise_at(vars(simpson), funs(mean(., na.rm=TRUE)))

std.error.simpson <- mastertable.df %>%
  group_by(site) %>%
  summarise_at(vars(simpson), funs(std.error(., na.rm=TRUE)))

# Evenness
mean.even <- mastertable.df %>%
  group_by(site) %>%
  summarise_at(vars(evenness), funs(mean(., na.rm=TRUE)))

std.error.even <- mastertable.df %>%
  group_by(site) %>%
  summarise_at(vars(evenness), funs(std.error(., na.rm=TRUE)))

# Total
mean.H.total <- mastertable.df %>%
  group_by(e.w) %>%
  summarise_at(vars(H), funs(mean(., na.rm=TRUE)))

std.error.H.total <- mastertable.df %>%
  group_by(e.w) %>%
  summarise_at(vars(H), funs(std.error(., na.rm=TRUE)))

mean.simpson.tot <- mastertable.df %>%
  group_by(e.w) %>%
  summarise_at(vars(simpson), funs(mean(., na.rm=TRUE)))

std.error.simpson.tot <- mastertable.df %>%
  group_by(e.w) %>%
  summarise_at(vars(simpson), funs(std.error(., na.rm=TRUE)))

mean.even.tot <- mastertable.df %>%
  group_by(e.w) %>%
  summarise_at(vars(evenness), funs(mean(., na.rm=TRUE)))

std.error.even.tot <- mastertable.df %>%
  group_by(e.w) %>%
  summarise_at(vars(evenness), funs(std.error(., na.rm=TRUE)))

# Test for normality
shapiro.test(H)
shapiro.test(simpson)
shapiro.test(evenness)

leveneTest(H ~ site, data = mastertable.df)
leveneTest(simpson ~ site, data = mastertable.df)
leveneTest(evenness ~ site, data = mastertable.df)

# Kruskal-Wallis tests
kruskal.test(H ~ site, data = mastertable.df)
kruskal.test(simpson ~ site, data = mastertable.df)
kruskal.test(evenness ~ site, data = mastertable.df)

# Dunn test
dunn.test(mastertable.df$H, g=mastertable.df$site)
dunn.test(mastertable.df$simpson, g=mastertable.df$site)
dunn.test(mastertable.df$evenness, g=mastertable.df$site)


# Boxplots
p2 <- ggplot(data=mastertable.df, aes(x=site, y=H, fill=site)) +
```

```
  geom_boxplot()
p2 <- p2 + theme_classic()
p2 <- p2 + labs(x="", y="H")
p2 <- p2 + scale_x_discrete(labels= c("Barite field", "Eastern mound",
"Eastern periphery", "Western mound", "Western periphery"))
p2 <- p2 + theme(legend.position = "none")
p2 <- p2 + theme(axis.text.x = element_text(size=12),
axis.text.y = element_text(size=12), axis.title = element_text(size = 13))
p2

p2 <- ggplot(data=mastertable.df, aes(x=site, y=simpson, fill=site)) +
  geom_boxplot()
p2 <- p2 + theme_classic()
p2 <- p2 + labs(x="", y="Simpson")
p2 <- p2 + scale_x_discrete(labels= c("Barite field", "Eastern mound",
"Eastern periphery", "Western mound", "Western periphery"))
p2 <- p2 + theme(legend.position = "none")
p2 <- p2 + theme(axis.text.x = element_text(size=12),
axis.text.y = element_text(size=12), axis.title = element_text(size = 13))
p2

p2 <- ggplot(data=mastertable.df, aes(x=site, y=evenness, fill=site)) +
  geom_boxplot()
p2 <- p2 + theme_classic()
p2 <- p2 + labs(x="", y="Evenness")
p2 <- p2 + scale_x_discrete(labels= c("Barite field",
"Eastern mound", "Eastern periphery",
 "Western mound", "Western periphery"))
p2 <- p2 + theme(legend.position = "none")
p2 <- p2 + theme(axis.text.x = element_text(size=12),
axis.text.y = element_text(size=12),
axis.title = element_text(size = 13))
p2

# Matrix for correltions
corr.subset <- c("qflux", "temp", "roughness", "slope", "northness", "eastness",
"act_brown", "act_small", "amphipod", "eelpout", "shrimp",
"snail", "sponge", "tw_area"  )
correlations.df <- mastertable.df[corr.subset]

correlations.matrix <- data.matrix(correlations.df, rownames.force = NA)

# Spearman's correlations

spear.corr <- rcorr(correlations.matrix, type=c("spearman"))


# GAM

attach(mastertable.df)
gam1 <- gam(total ~ s(temp) + s(slope), method = "REML")

ggplot(mastertable.df, aes(total, temp + qflux + slope + roughness
+ northness + eastness ))
+ geom_point() + geom_smooth(method = "gam", formula = y ~s(x))

gam.check(gam1)
summary(gam1)
plot(gam1, pages=1, rug=TRUE)

concurvity(gam1, full = TRUE)
concurvity(gam1, full = FALSE)

```

```
# Actiniaria small
attach(mastertable.df)
gam2 <- gam(act_small ~ s(temp) + s(slope), method = "REML")
gam.check(gam2)
summary(gam2)
plot(gam2, pages=1, rug=TRUE)

# Actiniaria brown
attach(mastertable.df)
gam3 <- gam(act_brown ~ s(temp) + s(slope), method = "REML")
gam.check(gam3)
summary(gam3)
plot(gam3, pages=1, rug=TRUE)

# Amphipods
attach(mastertable.df)
gam4 <- gam(amphipod ~ s(temp) + s(slope), method = "REML")
gam.check(gam4)
summary(gam4)
plot(gam4, pages=1, rug=TRUE)

# Eelpout
attach(mastertable.df)
gam5 <- gam(eelpout ~ s(temp) + s(slope), method = "REML")
gam.check(gam5)
summary(gam5)
plot(gam5, pages=1, rug=TRUE)

# Bythocaris
attach(mastertable.df)
gam6 <- gam(shrimp ~ s(temp) + s(slope), method = "REML")
gam.check(gam6)
summary(gam6)
plot(gam6, pages=1, rug=TRUE)

# Buccinidae
attach(mastertable.df)
gam7 <-gam(snail ~ s(temp) + s(slope), method = "REML")
gam.check(gam7)
summary(gam7)
plot(gam7, pages=1, rug=TRUE)

# Porifera
attach(mastertable.df)
gam8 <- gam(sponge ~ s(temp) + s(slope), method = "REML")
gam.check(gam8)
summary(gam8)
plot(gam8, pages=1, rug=TRUE)


# Sclerolinum contortum
attach(mastertable.df)
gam9 <- gam(tw_area ~ s(temp) + s(slope), method = "REML")
gam.check(gam9)
summary(gam9)
plot(gam9, pages=1, rug=TRUE)


# Species richness (no. of species)
attach(mastertable.df)
gam10 <- gam(sp.no ~ s(temp) + s(slope), method = "REML")
gam.check(gam10)
summary(gam10)
```

```r
plot(gam10, pages=1, rug=TRUE)


# Boxplot
p2 <- ggplot(data=correlations.df, aes(x=site, y=H, group=site)) +
  geom_boxplot()
p2

# nMDS
# Matrix

counts2.df <- counts.df[c(-1,-2,-3)]

counts.matrix <- data.matrix(counts2.df, rownames.force = NA)

#distance matrix
count_distmat <- vegdist(counts.matrix, method = "bray")
count_distmat <- as.matrix(counts.matrix, labels = T)


density_NMS <- metaMDS(count_distmat, distance="bray", k=3, maxit=999,
trymax=500, noshare= 0.1, wascores=TRUE)

stressplot(density_NMS) # Produces a Shepards diagram


# Plotting NMDS with ggplot
data.scores = as.data.frame(scores(density_NMS))
data.scores$site = counts.df$site

p13 <- ggplot(data= data.scores, aes(x=NMDS1, y=NMDS2, colour=site)) +
  geom_point()
p13 <- p13 + theme_classic()
p13 + scale_color_manual(name = "Site", labels= c("Barite field", "Eastern mound",
"Eastern periphery", "Western mound", "Western periphery"))
p13 <- p13 + stat_ellipse(aes(x=NMDS1,y=NMDS2),level = 0.50)
p13

# PERMANOVA

distmat_transformed <- wisconsin(count_distmat)
distmat_transformed2 <- sqrt(distmat_transformed)
adon.results<-adonis(distmat_transformed2 ~ counts.df$site, method="bray",perm=999)
print(adon.results)

# pairwise adonis
pairwise.adonis <- function(x,factors, sim.method = 'bray', p.adjust.m ='bonferroni')
{
  library(vegan)
  co = combn(unique(factors),2)
  pairs = c()
  F.Model =c()
  R2 = c()
  p.value = c()
  for(elem in 1:ncol(co)){
    ad = adonis(x[factors %in% c(co[1,elem],co[2,elem]),]
    ~ factors[factors %in% c(co[1,elem],co[2,elem])] , method =sim.method);
    pairs = c(pairs,paste(co[1,elem],'vs',co[2,elem]));
    F.Model =c(F.Model,ad$aov.tab[1,4]);
    R2 = c(R2,ad$aov.tab[1,5]);
    p.value = c(p.value,ad$aov.tab[1,6])
  }
  p.adjusted = p.adjust(p.value,method=p.adjust.m)
```

```
  pairw.res = data.frame(pairs,F.Model,R2,p.value,p.adjusted)
  return(pairw.res)
}

par.adonis.test <- pairwise.adonis(distmat_transformed2, counts.df$site1,
sim.method = 'bray', p.adjust.m ='bonferroni')
print(par.adonis.test)

# SIMPER

simper.test <- simper(distmat_transformed2, counts.df$site,
permutations = 0, trace = FALSE,
       parallel = getOption("mc.cores"))

summary(simper.test, ordered = TRUE,
        digits = max(3,getOption("digits") - 3))
```

C. Morphospecies distribution maps

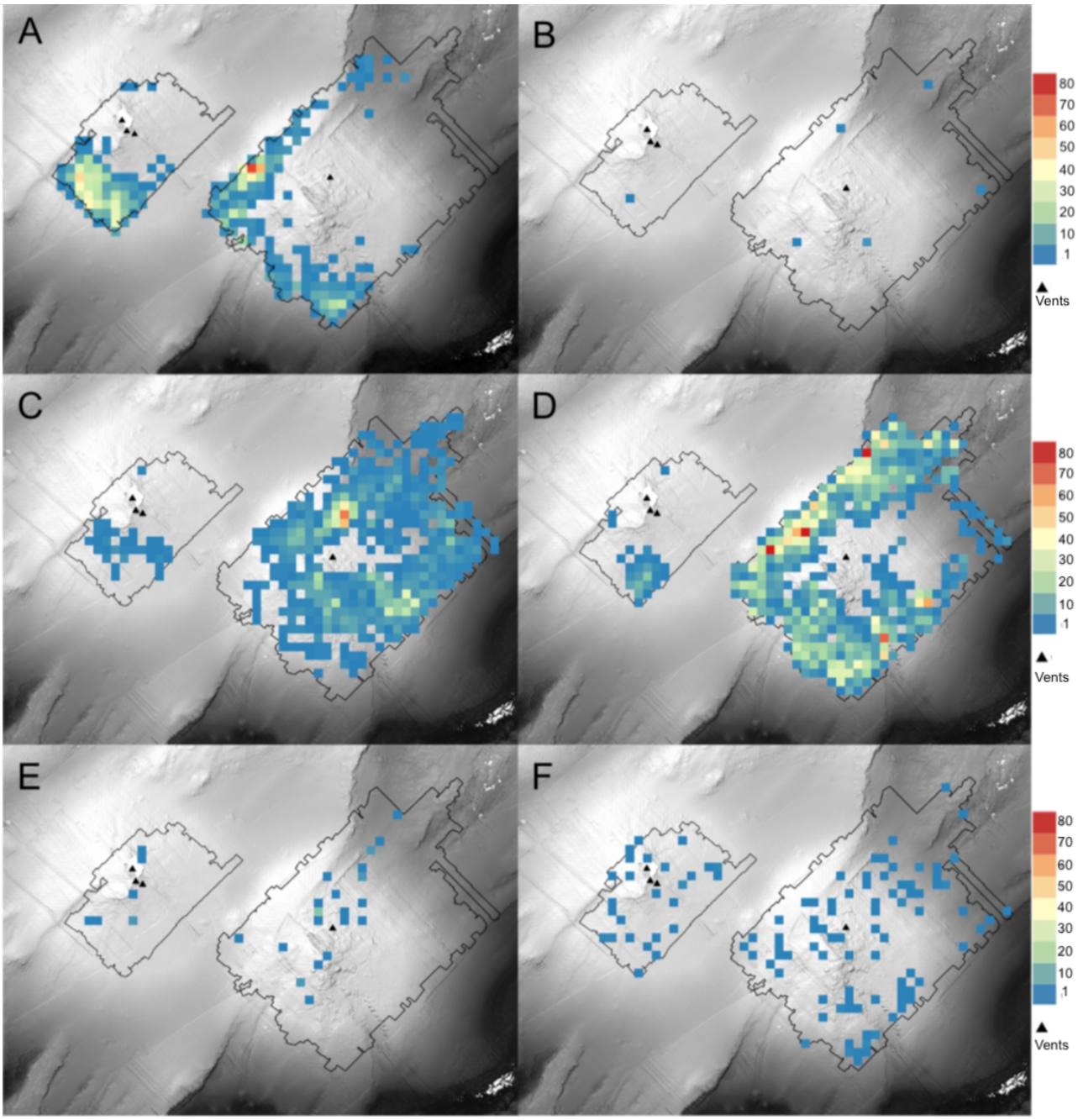

Figure C.1: Abundance of A) Porifera indet. 1., B) Cladorhizidae indet., C) Actiniaria stet. 1, D) Actiniaria stet.. 2, E) Actiniaria stet. 3, F) *Crossata* sp. indet. and Narcomedusae indet. Each pixel represents 5x5m. The figure continues on the next page.

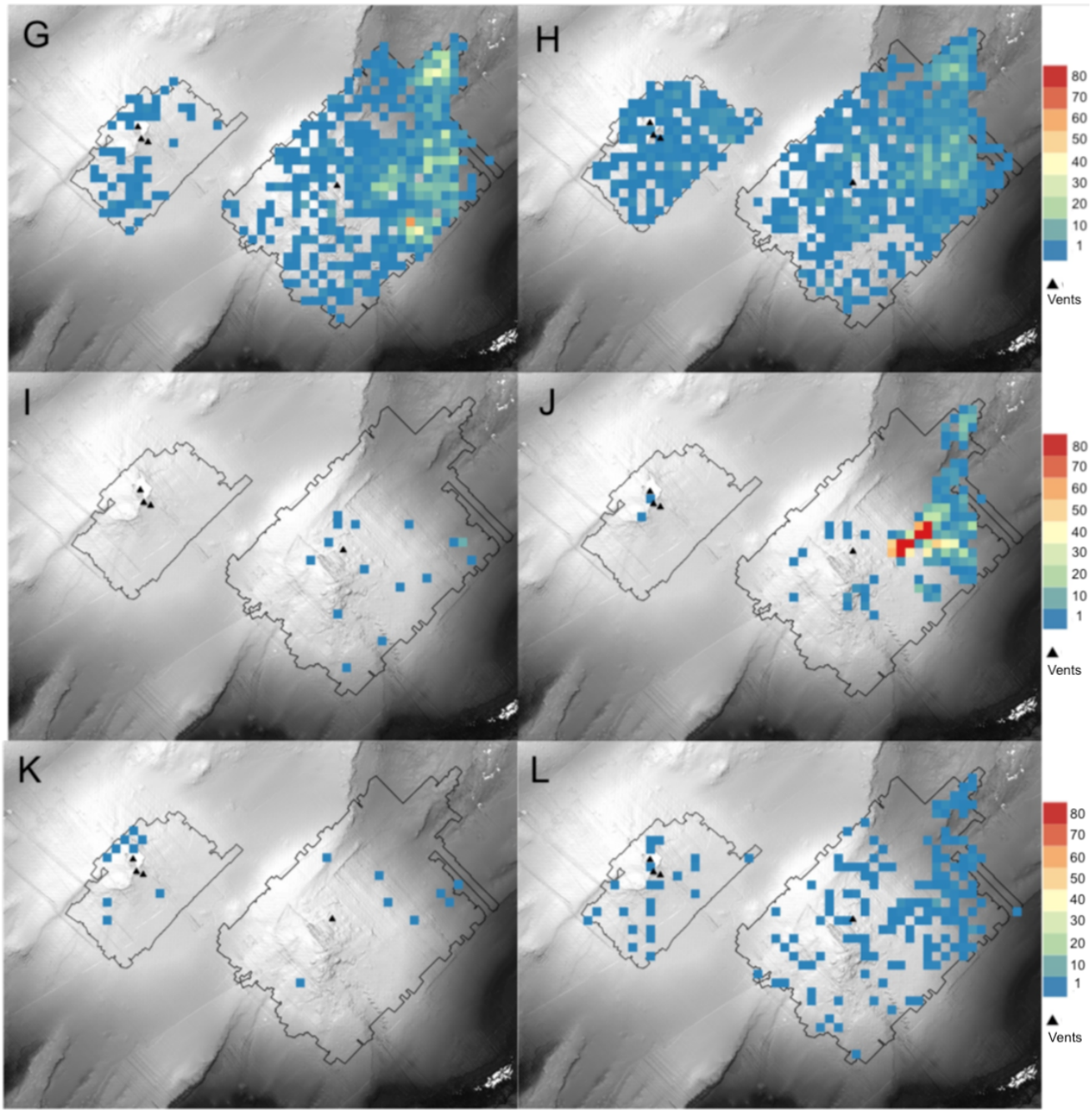

Figure C.2: Continued from previous page. Abundance of G) Buccinidae indet., H) *Bythocaris* sp. indet., I) Munnopsidae stet., J) Amphipoda stet., K) Echinodermata, L) *Lycenchelys platyrhina*. Each pixel represents 5x5m.

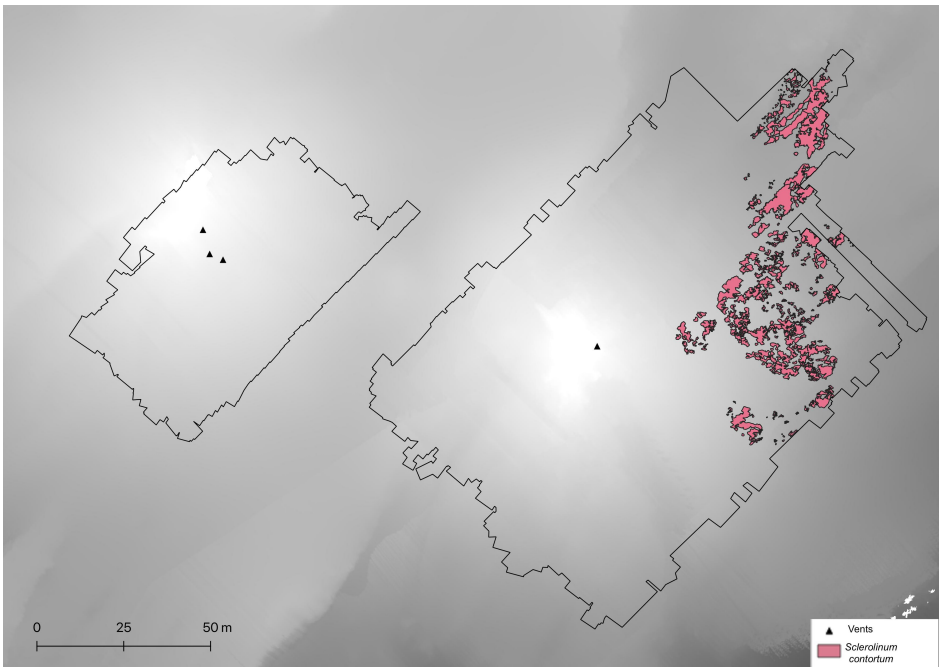

Figure C.3: Coverage of *Sclerolinum contortum* colonies.

D. Smoothing curves from GAMs

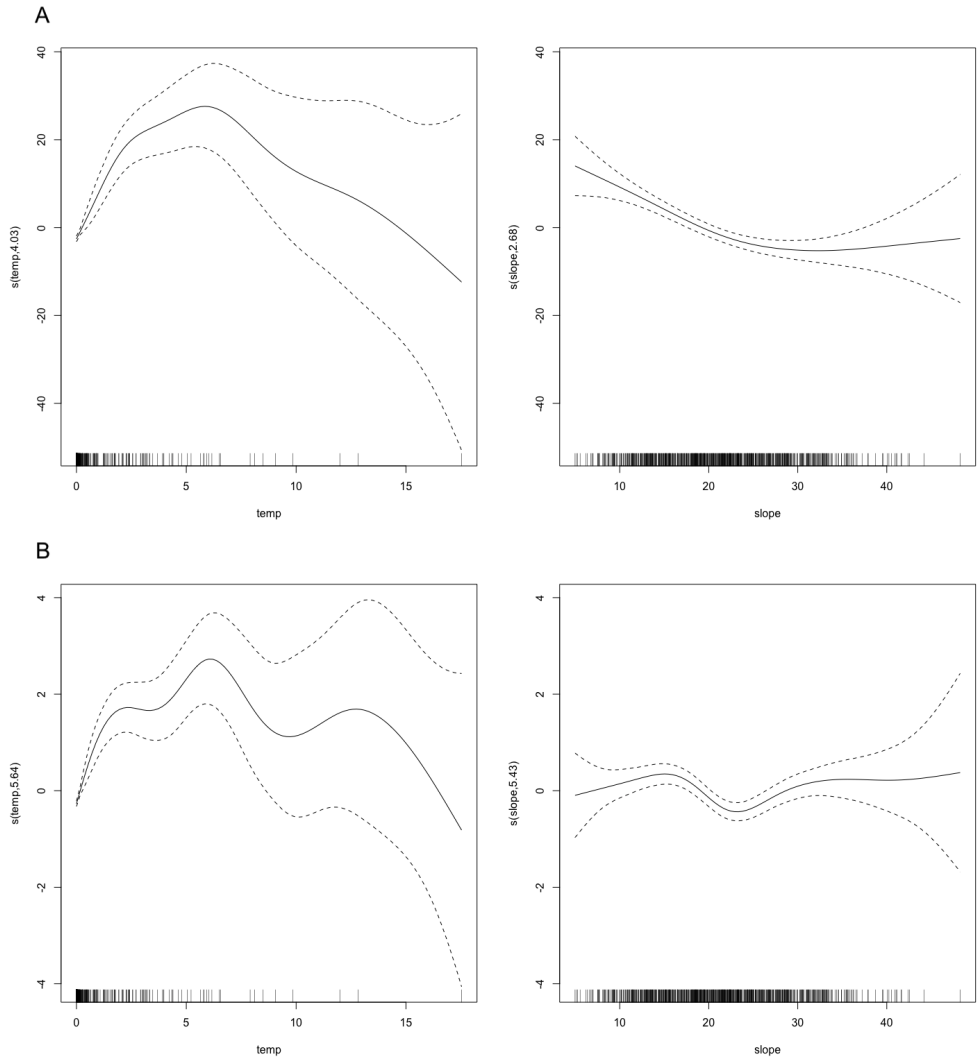

Figure D.1: Smoothing curves of a) Total abundance, b) Species richness (S).

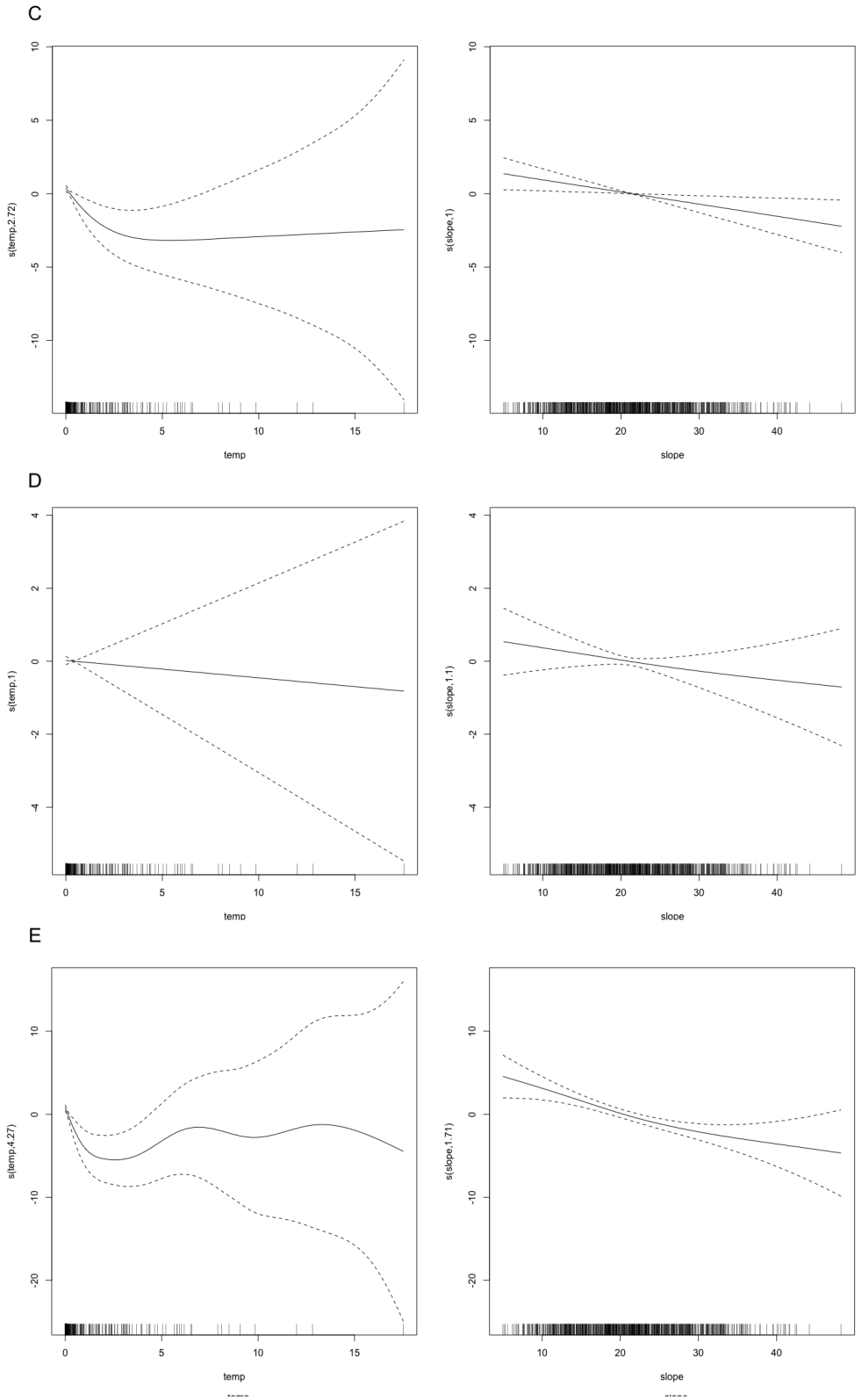

Figure D.2: Smoothing curves of c) Porifera indet. 1, d) Actiniaria stet. 1, e) Actiniaria stet. 2

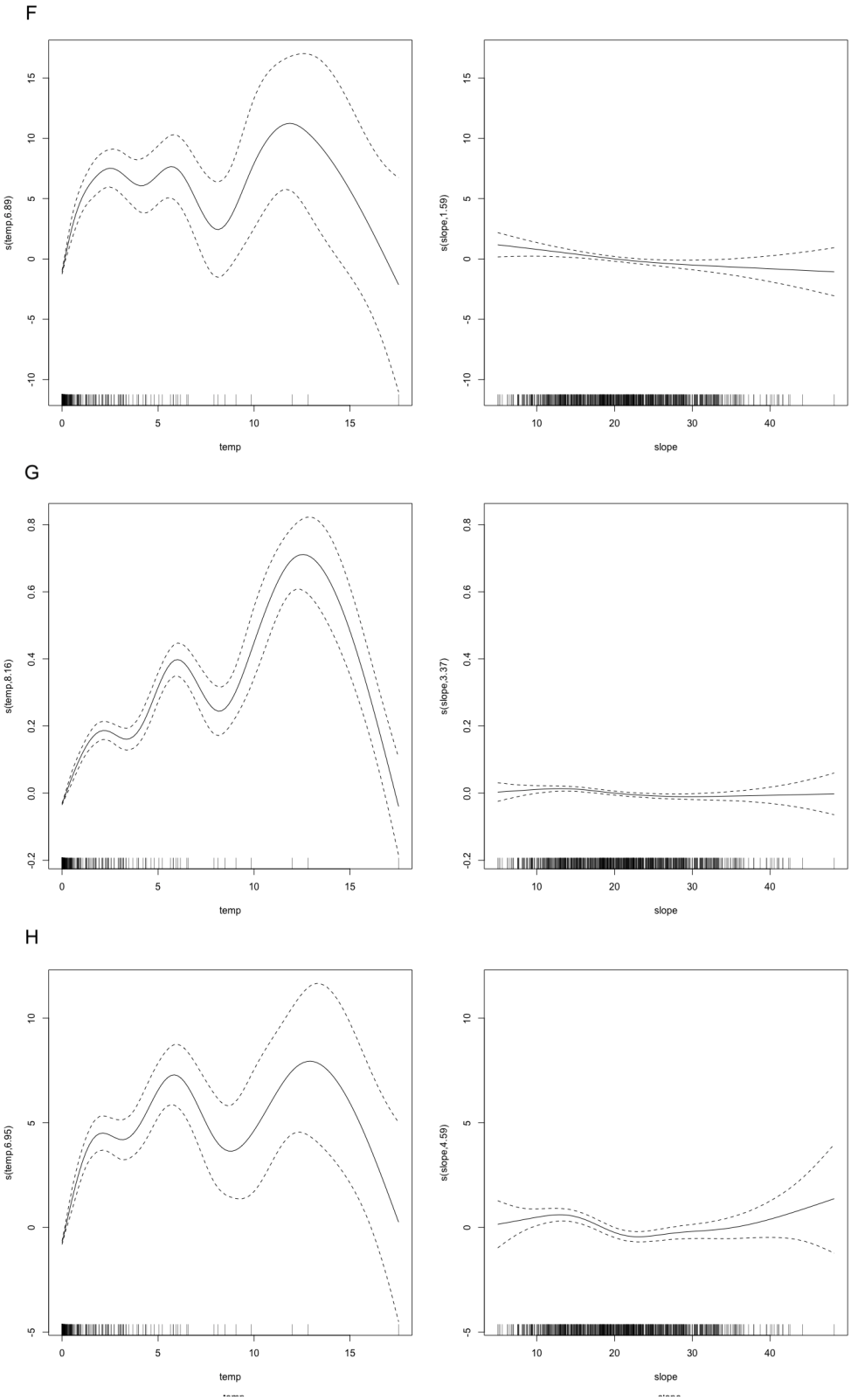

Figure D.3: Smoothing curves of f) Buccinidae indet., g) *Sclerolinum contortum*, h) *Bythocaris* sp. indet.

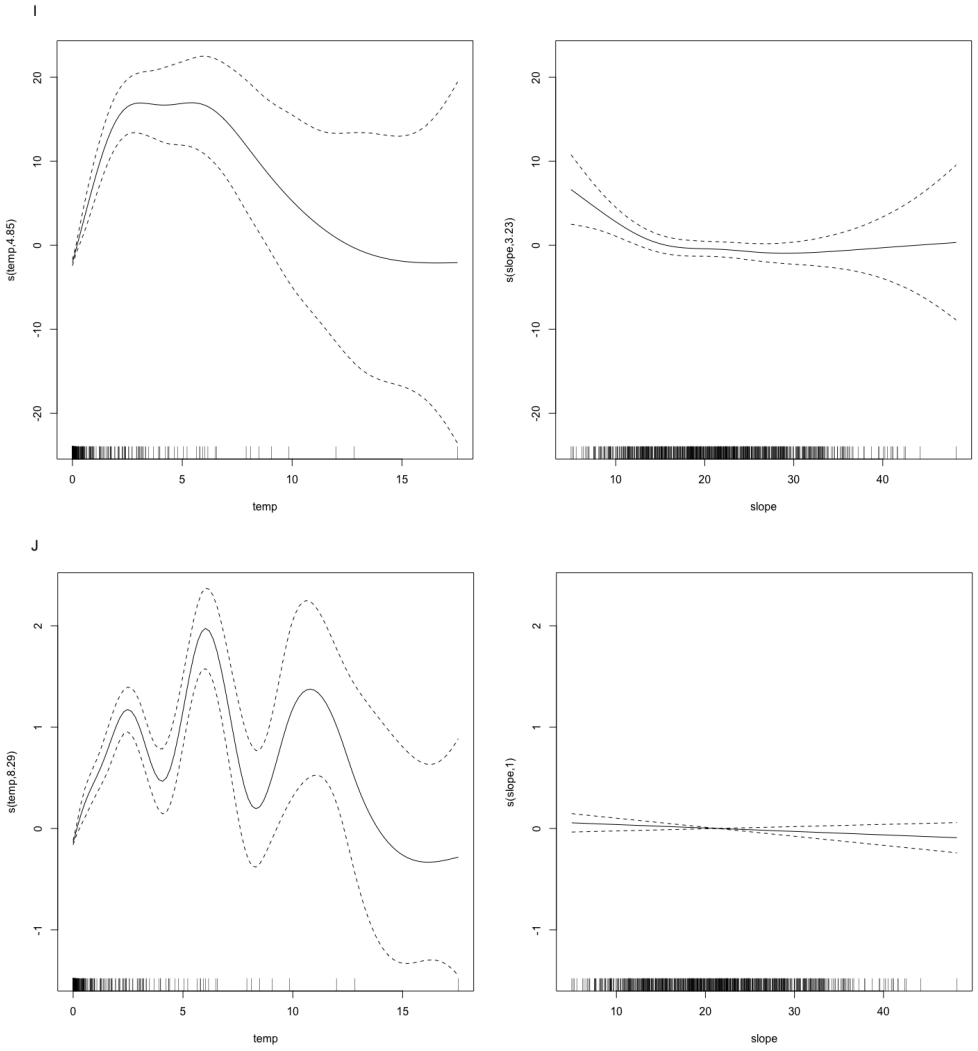

Figure D.4: Smoothing curves of i) Amphipoda stet., j) *Lycenchelys platyrhina*.